IX. VIBRATIONAL SPECTROSCOPY

1. Diatomic molecules

a) Energy levels and selection rules

We have already seen that in general, the vibrational energy levels of a diatomic molecule can be expressed as

$$G(v) \;=\; \omega_e(v+1/2) - \omega_e x_e(v+1/2)^2 + \omega_e y_e(v+1/2)^3 + ... \tag{9.1}$$

The first term in (9.1) is the harmonic oscillator term, and the higher order terms result from anharmonicity. The constants $\omega_e x_e$, $\omega_e y_e$,... are the anharmonic constants, and cause the higher v levels to be closer together than the lower v levels (see Figure 7.2). For example, for $^1H^{35}Cl$, $\omega_e x_e = 52.8186$ cm^{-1}, $\omega_e y_e = 0.2244$ cm^{-1} and $\omega_e z_e = -0.0122$ cm^{-1}. A useful summary of these constants has been given by Huber and Herzberg, 1977 "Constants of Diatomic Molecules".

The strength of a transition between two vibrational states v' and v'' is again proportional to the square of the transition moment R_v:

$$R_v = < v'|\vec{\mu}|v'' > \tag{9.2}$$

where μ is the dipole moment defined in Equation (8.16). The dipole moment can be expanded in a Taylor series around the equilibrium distance R_e:

$$\vec{\mu} = \vec{\mu}_e + \left(\frac{d\vec{\mu}}{dR}\right)_{R_e}(R-R_e) + \frac{1}{2}\left(\frac{d^2\vec{\mu}}{dR^2}\right)_{R_e}(R-R_e)^2 + ... \tag{9.3}$$

so that R_v becomes:

$$R_v = \vec{\mu}_e < v'|v'' > + \left(\frac{d\vec{\mu}}{dR}\right)_{R_e} < v'|R-R_e|v'' > + ... \tag{9.4}$$

Since the vibrational functions $\Psi^{v'}$ and $\Psi^{v''}$ are eigenfunctions of the same Hamiltonian, they are orthogonal for $v' \neq v''$:

$$< v'|v'' > = \delta_{v'v''} \tag{9.5}$$

so that the leading term of Equation (9.4) is, without approximation,

$$R_v = \left(\frac{d\vec{\mu}}{dR}\right)_{R_e} < v'|R-R_e|v'' > . \tag{9.6}$$

Thus, the strength of a vibrational band in the infrared depends on the magnitude of the *derivative* of the dipole moment with internuclear distance. Figure 9.1 shows how the dipole moment μ varies with R in a typical heteronuclear diatomic molecule. Obviously, $\mu \to 0$ when $R \to 0$, since the nuclei coalesce. For neutral diatomics, $\mu \to 0$ when $R \to \infty$

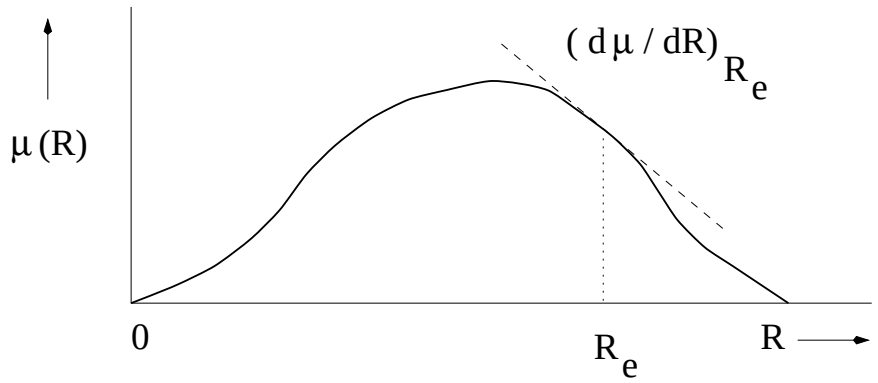

Figure 9.1– Variation of dipole moment with internuclear distance in a heteronuclear diatomic molecule.

because the molecule dissociates into neutral atoms. Therefore, between $R = 0$ and ∞, there must be a maximum value of μ. In Figure 9.1, this maximum occurs at $R < R_e$, giving a negative slope $\mathrm{d}\mu/dR$ at R_e. If the maximum were at $R > R_e$, there would be a positive slope at R_e.

A molecule with a relatively small dipole moment may still have a large dipole derivative, and, conversely, a molecule with a very large dipole moment may have a small dipole derivative if the dipole moment is near its maximum value at $R = R_e$, so that $d\mu/dR$=0 at R_e. For example, CO, which has a permanent moment of only 0.11D, possesses a large dipole derivative, and thus one of the strongest known infrared absorptions. A homonuclear molecule, however, for which μ=0 at all internuclear separations, has a dipole derivative that is zero everywhere, and thus no electric dipole vibrational absorption at all. Thus, homonuclear molecules such as H_2, O_2 and N_2 have neither vibrationally nor rotationally electric dipole allowed transitions.

In the pure harmonic oscillator approximation, only $\Delta v = v' - v'' = \pm 1$ transitions can occur. For real, anharmonic molecules, there is no selection rule on the change in vibrational quantum number v, although the $\Delta v = \pm 1$ transitions always have vastly larger probabilities than $\Delta v > 1$ transitions. Transitions with $\Delta v = \pm 1$ are called "fundamental bands", whereas those with $\Delta v = \pm 2, \pm 3, ...$ are called "overtone bands".

b) Vibration-rotation spectroscopy

Associated with each vibrational level is a stack of rotational energy levels, as shown, for example, in Figure 7.5. In the rotational spectroscopy discussed in § VIII, we considered transitions between rotational energy levels associated with the same vibrational level (usually v=0). In vibration-rotation spectroscopy, we consider transitions between the sets of rotational energy levels associated with two different vibrational levels. Thus, a vibrational "band", that is a transition $v' \leftrightarrow v''$, is composed of a number of "lines" $v'J' \leftrightarrow v''J''$. The energy levels are given by the sum of the rotational term values $F_v(J)$ and the vibrational term values $G(v)$

$$E^{vr} = G(v) + F_v(J) = \omega_e(v+1/2) - \omega_e x_e(v+1/2)^2 + ... + B_v J(J+1) - D_v J^2(J+1)^2 \quad (9.7)$$

Figure 9.2 illustrates the rotational levels associated with two vibrational levels v' and v''. The selection rules on rotational quantum number, parity etc.. derived in § VIII still

apply. Thus, in addition to the vibrational selection rules, we have

$$\Delta J = \pm 1. \tag{9.8}$$

The selection rule $\Delta J = \pm 1$ holds strictly only for a molecule in a Σ state. Transitions with ΔJ=0 can occur when the electronic angular momentum of the molecule is non-zero.

The "band origin" is the mythical place where the $J' = J'' = 0$ transition would occur, if it were not forbidden. The vibrational band is then composed of a number of 'branches', which in the simplest case are:

$$\begin{array}{ll} \text{R-branch:} & \Delta J = J' - J'' = +1 \\ \text{Q-branch:} & \Delta J = 0 \\ \text{P-branch:} & \Delta J = J' - J'' = -1 \end{array} \tag{9.9}$$

Note that the Q branch transitions do not occur for Σ states. The frequencies of each of the lines are

$$\begin{aligned} \tilde{\nu}_P(J) &= \tilde{\nu}_0 + B'J'(J'+1) - B''J''(J''+1) \\ &= \tilde{\nu}_0 + B'(J-1)J - B''J(J+1) \\ &= \tilde{\nu}_0 - (B'+B'')J + (B'-B'')J^2. \end{aligned} \tag{9.10}$$

Similarly:

$$\tilde{\nu}_R(J) = \tilde{\nu}_0 + (B'+B'')(J+1) + (B'-B'')(J+1)^2. \tag{9.11}$$

The appearance of such a vibration-rotation band is also indicated in Figure 9.2, together with the actual v=1-0 spectrum of the HCl molecule. The band appears fairly symmetrical about the band center ν_0, and there is approximately equal spacing between adjacent R-branch lines, and between adjacent P-branch lines, but there is twice as large a space between the first R and P branch lines, R(0) and P(1). This spacing between R(0) and P(1) is called the zero gap, and it is in this region where the band origin ν_0 falls. Also, the Q branch, if present, would occur in this gap.

The approximate symmetry of the band is due to the fact that $B' \approx B''$, that is, the vibration-rotation interaction constant α in Eq. (7.52a) is small. Then:

$$\begin{aligned} \tilde{\nu}_P &= \tilde{\nu}_0 - 2BJ \\ \tilde{\nu}_R &= \tilde{\nu}_0 + 2B(J+1) \end{aligned} \tag{9.12}$$

so that the zero gap $\tilde{\nu}(R(0) - P(1)) = 4B$.

A closer look at the HCl spectrum in Figure 9.2 reveals that the bands are not quite symmetrical, but show a convergence in the R branch and a divergence in the P branch, resulting from the fact that B' and B'' are not quite equal. The observed energy levels can then be used to determine these two quantities separately.

When individual levels must be labelled with both N and J quantum numbers, then there can be two R-branch lines for each value of J'', two Q-branch lines for each J'', and so on. In cases where $\Lambda > 1$ ($\Pi, \Delta, ...$ states), each of these lines is further split into two closely-spaced lambda components. Note that the selection rule $\Delta J = 0, \pm 1$ and the

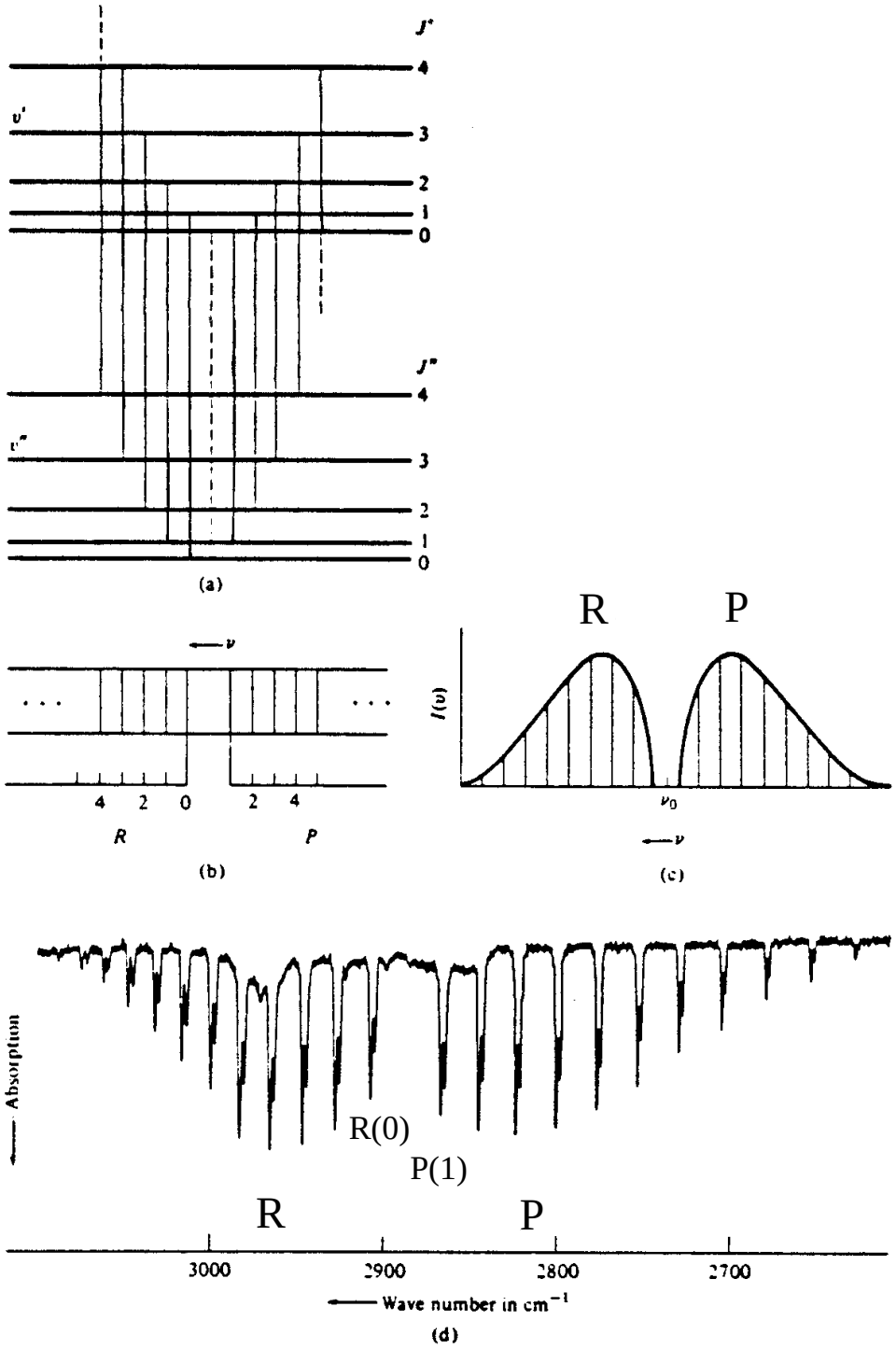

Figure 9.2– Structure of a vibration-rotation band: (a) Rotational energy levels associated with upper and lower vibrational energy levels, and allowed transitions; (b) Spectral lines for the transition; (c) Intensity distribution over the spectrum; (d) Actual infrared absorption spectrum of HCl (Note: The splitting of each line is due to the presence of both $H^{35}Cl$ and $H^{37}Cl$ in the gas cell).

approximate selection rule $\Delta N = 0, \pm 1$ need not be satisfied in the same way at the same time; thus it is possible to have additional 'satellite' branches. For example, look at the structure of a $^2\Sigma$ band:

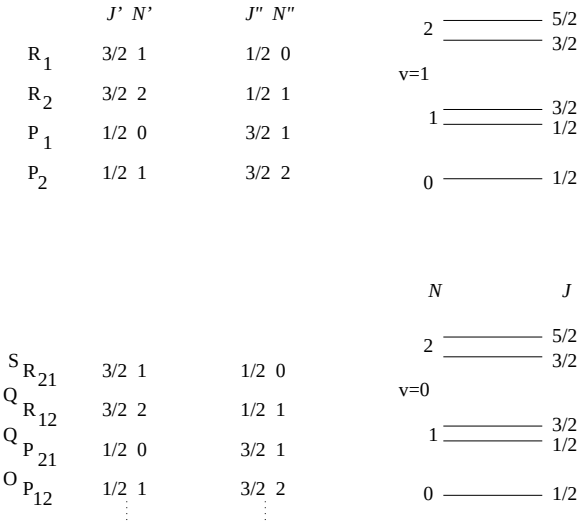

The superscripts indicate the change in N when this is not the same as the change in J; note that $\Delta N \pm 2$ is possible, where the S- and O- branches refer to $N' - N'' = +2$ and $N' - N'' = -2$, respectively. S- and O- branches also occur in quadrupole transitions where $\Delta J = \pm 2, 0$.

The intensity distribution among rotational transitions in a vibration-rotation band is governed again by the Boltzmann distribution; the same holds for the distribution over the various vibrational levels. Table 9.1 illustrates that at low temperatures, virtually all molecules are in the lowest vibrational level, so that in astrophysical regions with $T \leq 1000K$, one expects to observe only lines involving the lowest vibrational levels.

Table 9.1– Ratio of the Populations of the Lowest Two Vibrational States of Selected Molecules

Gas	ν_1 (cm^{-1})	$\exp(-h\nu_1/k\theta)$ 300 K	$\exp(-h\nu_1/k\theta)$ 1000 K
H_2	4160.2	2.16×10^{-9}	2.51×10^{-3}
HCl	2885.9	9.77×10^{-7}	1.57×10^{-2}
N_2	2330.7	1.40×10^{-5}	3.50×10^{-2}
CO	2143.2	3.43×10^{-5}	4.58×10^{-2}
O_2	1556.4	5.74×10^{-4}	1.07×10^{-1}
Cl_2	556.9	6.92×10^{-2}	4.49×10^{-1}
I_2	213.2	3.60×10^{-1}	7.63×10^{-1}

c) Diatomic Examples

(i) H_2

The vibration-rotation spectrum of H_2 is observed in a wide variety of astrophysical regions, ranging from hot, star-forming clouds and planetary nebulae, to planetary atmospheres. The electronic ground state of H_2 is X $^1\Sigma_g^+$, so that the vibration-rotation

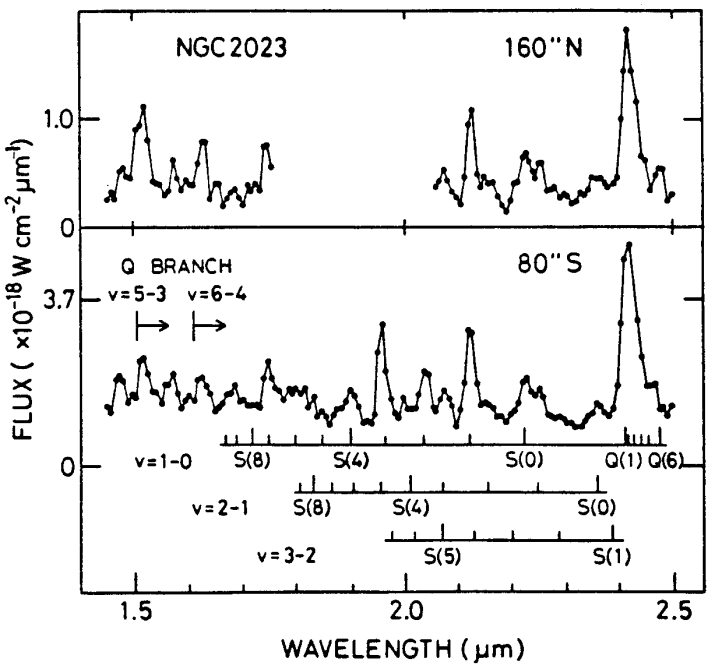

Figure 9.3– Infrared emission spectrum of H_2 from the reflection nebula NGC 2023 (from: Gatley *et al.* 1987)

spectrum is relatively simple. However, the molecule has no permanent dipole moment, so that only quadrupole transitions can occur for which $\Delta J = 0, \pm 2$. Thus, the spectrum is composed of S, Q and O branches. In the $v' = 1 \Leftrightarrow v'' = 0$ band, the S lines occur around 2.7-2.9μm. Lines in the $2 \leftrightarrow 1$ and $3 \leftrightarrow 2$ bands are shifted to slightly longer wavelengths. The atmospheric K-band window extends from about 2.05-2.45 μm, so that the S- and Q-branch lines can be observed from Earth, but not the O-branch lines. The strongest lines observed are the (v', v'')=(1,0) S(1) line at 2.12 μm, the (1,0) S(0) line at 2.22μm, the (2,1) S(1) line at 2.25μm and the (1,0) Q(1), Q(2) and Q(3) lines at 2.4μm. Several of these lines can be seen in the spectrum of NGC7027, presented in the introductory lecture. Another example of the H_2 vibration-rotation spectrum in a warm, dense cloud is shown in Figure 9.3. The relative strengths of these lines depend on the excitation mechanism.

If the excitation is thermal at $T \approx$2000 K (that is, collisional excitation dominates), the (2,1) S(1) line is usually much weaker than the (1,0) S(0) line. On the other hand, UV pumping, in the case of planetary atmospheres, can preferentially populate the higher vibrational levels, so that they appear relatively strongly in the spectrum. Thus, the relative strengths of the lines are an excellent diagnostic of the physical conditions such as temperature, density and/or strength of incident radiation field.

(ii) OH

Another familiar example of a vibration-rotation band system is the far-red and near-infrared airglow emission produced by the Earth's atmosphere, and seen in the introduction and Figure 6.27. These are the "Meinel bands" of OH named after Adam Meinel who identified them in 1950. A number of different bands in several different sequences (that

is, values of Δv) are seen:

(v', v'')=(6,0),(7,1),...(9,3)
(5,0),(6,1),...(9,4)
(4,0),(5,1),...(9,5)
(3,0),(4,1),...(9,6)
(2,0),(3,1),...(9,7)

No emission is seen with $v' > 9$. The reason for this is that the vibrationally-excited OH is produced by

$$H + O_3 \rightarrow OH + O_2 \tag{9.13}$$

in the upper atmosphere (90 km), and that at atmospheric temperatures this reaction is exothermic by 3.30 eV, that is, it releases a maximum amount of energy of 3.30 eV, which is just the energy of v=9 above the ground state! Thus, the reaction that forms OH also converts chemical energy into internal, vibrational energy of the product molecule.

Note that the observed emission also gives us information about the density at the altitude where H and O_3 are present, since the OH lines are not collisionally quenched.

2. Polyatomic Molecules

a) Group vibrations

An N-atomic molecule has 3N-5 independent modes of vibration if it is linear, and 3N-6 if it is non-linear. These vibrations are usually described in terms of "normal" modes, which belong to one of the symmetry types or "representations" of the symmetry group of the molecule. The form of the normal vibrations may be obtained from the internal coordinates of the molecule, such as bond lengths, angles, bond-stretching and angle-bending force constants, but the calculations are very complex and will not be given here. See, for example, Steinfeld Ch. 9, or Wilson, Decius and Cross, for more details.

The normal modes can be illustrated pictorially with vectors attached to the nuclei which indicate the directions and relative magnitudes of the motions. For example, the 3 normal modes of H_2O are illustrated in Figure 9.4. The first one, denoted as ν_1, is the "symmetric stretch". The second vibration, ν_2, is the "bending" motion, whereas the third mode, ν_3, is the "antisymmetric stretch". If we consider their behavior under the various symmetry operations of the group, we find that both ν_1 and ν_2 have A_1 symmetry, whereas ν_3 is of B_2 symmetry type.

For a linear triatomic molecule XY_2 such as CO_2, the normal modes are illustrated in Figure 9.5. Again, there are three modes ν_1 (symmetric stretch), ν_2 (bending) and ν_3 (antisymmetric stretch), but in this case the bending mode is "doubly degenerate" because there are two orthogonal planes in which the bending can occur. For a symmetric linear molecule XY_2, ν_1 has symmetry type Σ_g^+, while ν_3 has symmetry type Σ_u^+ and the degenerate mode has type Π_u. In unsymmetrical linear molecules XYZ, the g/u symmetry distinction between ν_1 and ν_3 stretching vibrations disappears: both are of symmetry Σ^+. For a general N-atom linear molecule, there are N-1 stretching modes and N-2 doubly degenerate bending modes.

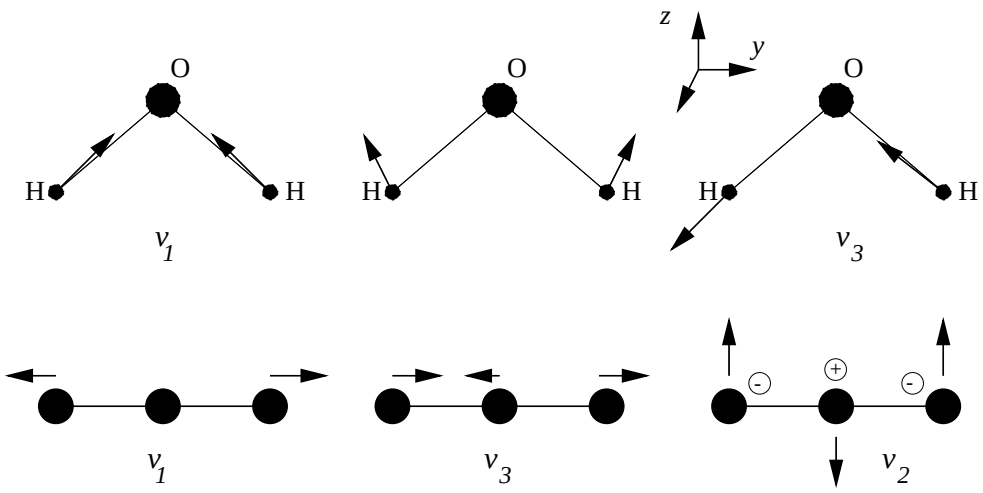

Figure 9.4– (Top) The normal modes of H_2O. **Figure 9.5**– (Bottom) The normal modes of a linear XY_2 molecule.

To a first approximation, vibrational energy levels can be described in terms of independent harmonic oscillators

$$G(v_1, v_2, ...) = \sum_i (\omega_i + d_i/2) \tag{9.14}$$

where ω_i and v_i are the vibrational frequency and quantum number of the ν_i normal mode, respectively, and d_i is 1 or 2 depending on whether the mode is non-degenerate or doubly degenerate. Note that for polyatomic molecules, the possibility of "combination" transitions exist, in which more than one vibration is excited, as Figure 9.6 shows.

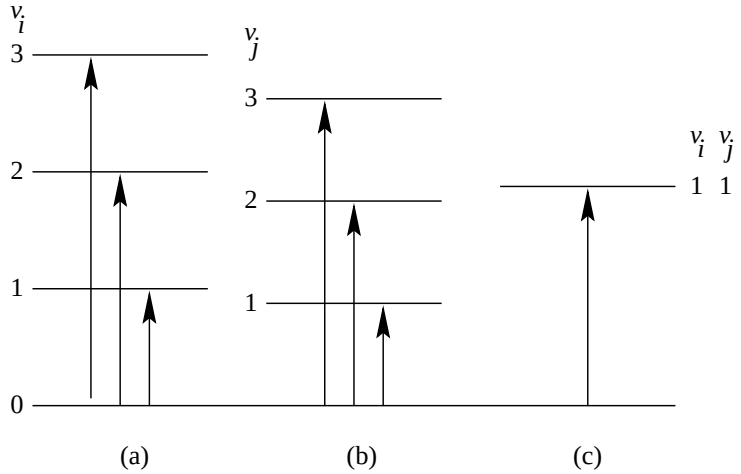

Figure 9.6– (a,b) Fundamental and overtone, and (c) combination transitions involving vibrations ν_i and ν_j.

b) Selection rules

As for a diatomic molecule, the general harmonic oscillator selection rule is $\Delta v_i = \pm 1$ for each vibrational mode, with $\Delta v_i = \pm 2, \pm 3, ...$ overtone transitions allowed, but generally weak, when anharmonicity is taken into account. In addition, there must be a change in the dipole moment for the transition to be electric dipole allowed.

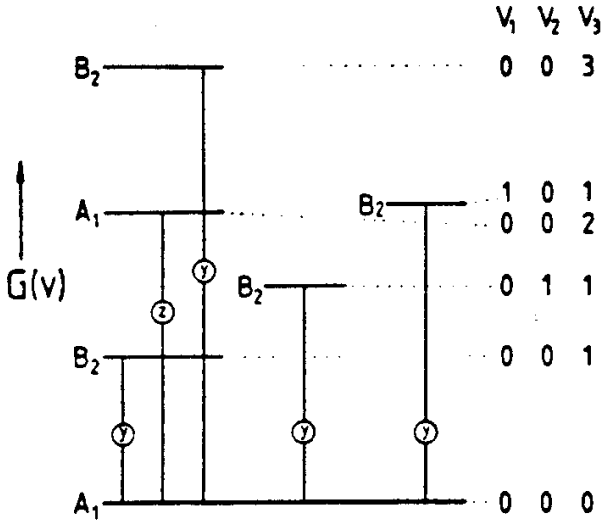

Figure 9.7– Symmetry species of some overtone and combination levels of H_2O together with the directions of the transition moments. The vibrational wavenumbers are $\tilde{\nu}_1 = 3657.1\ \mathrm{cm}^{-1}$, $\tilde{\nu}_2 = 1594.8\ \mathrm{cm}^{-1}$, $\tilde{\nu}_3 = 3755.8\ \mathrm{cm}^{-1}$.

In the case of H_2O, it is easy to see from the form of the normal modes that all vibrations ν_1, ν_2 and ν_3 involve a change of dipole moment and are "infrared active", that is, the $v = 1 - 0$ transition in each vibration is allowed. The transitions may be indicated as (v_1, v_2, v_3)=(1,0,0)$\leftrightarrow$(0,0,0); (0,1,0)$\leftrightarrow$(0,0,0) and (0,0,1)$\leftrightarrow$(0,0,0) or alternatively 1_0^1, 2_0^1 and 3_0^1 where $N_{v''}^{v'}$ refers to a transition with lower and upper state vibrational quantum number v'' and v', respectively, in vibration N. In the case of CO_2 on the other hand, only the modes ν_2 and ν_3 involve a change of dipole moment, so that transitions involving the symmetric stretch ν_1 are electric dipole forbidden or "infrared inactive".

Although for the cases of H_2O and CO_2 we can easily see which vibrational modes are infrared active, this is in general not the case, nor is it for overtone and combination band transitions. However, the selection rules follow very readily from symmetry arguments. The transition probability for a vibrational mode v_i is again proportional to the square of the transition moment

$$R_{v_i} = < v_i' | \mu | v_i'' > . \tag{9.15}$$

As explained in § VII.4c, this matrix element is only non-zero if the product of the symmetry types of $\Psi^{v'}, \Psi^{v''}$ and one of the components of the dipole operator μ_x, μ_y, μ_z is totally symmetric. In group theoretical notation:

$$\Gamma(\Psi^{v'}) \otimes \Gamma(\mu) \otimes \Gamma(\Psi^{v''}) = A_1 \tag{9.16}$$

where Γ stands for "symmetry type of" and A_1 denotes the totally symmetric representation. In the case of degenrate vibrations or symmetry types, the product needs to contain at least a totally symmetric part.

We can easily check that this is the case for the three vibrations in H_2O. Note that $\Psi^{v''} \leftrightarrow A_1$ if $v_1'' = v_2'' = v_3'' = 0$. Also we have seen in § VII that $\mu_x \leftrightarrow B_1$, $\mu_y \leftrightarrow B_2$ and $\mu_z \leftrightarrow A_1$. For the 1_0^1 transition, we then find

x-component: $A_1 \otimes B_1 \otimes A_1 = B_1 \neq A_1$: forbidden
y-component: $A_1 \otimes B_2 \otimes A_1 = B_2 \neq A_1$: forbidden
z-component: $A_1 \otimes A_1 \otimes A_1 = A_1 = A_1$: allowed!

Thus, the 1_0^1 transition can occur by z-polarized electric dipole radiation. Similarly, we find that the 2_0^1 transition can also occur by the z-component, whereas the 3_0^1 transition is allowed by y-polarized electric dipole radiation. Figure 9.7 illustrates some other overtone and combination tone transitions for H_2O.

c) Vibration-rotation spectroscopy

As for diatomic molecules, we also have to consider the set of rotational energy levels associated with each vibrational level. The resulting term values are given by the sum of the rotational and vibrational term values

$$E^{vr} = G(v_i) + F_{v_i}(J) \tag{9.17}$$

where the formulae for $F(J)$ have been discussed in § VIII.

(i) Linear molecules

For a symmetric, triatomic molecule such as CO_2, we have seen already that only the vibrational modes ν_2 and ν_3 are infrared active, where ν_2 is of symmetry type Π_u and ν_3 of type Σ_u^+. More generally, in such a symmetric linear polyatomic, only transitions between upper and lower states of the type

$$\Sigma_u^+ - \Sigma_g^+ \text{ and } \Pi_\mathrm{u} - \Sigma_\mathrm{g}^+ \tag{9.18}$$

are allowed. For an unsymmetrical triatomic molecule like HCN, all three modes can have electric dipole allowed transitions. More generally, the rule in this case is:

$$\Sigma^+ - \Sigma^+ \text{ and } \Pi - \Sigma^+. \tag{9.19}$$

For a $\Sigma - \Sigma$ transition, the rotational selection rule is again $\Delta J = \pm 1$, resulting in a spectrum with P and R branches. The P and R lines are separated by about $2B$, and there is a spacing of about $4B$ between R(0) and P(1).

For a $\Pi - \Sigma$ transition, the selection rule become $\Delta J = 0, \pm 1$, so that also Q branches can appear. In addition, the parity must change, $+ \leftrightarrow -$.

Figure 9.8 (top) shows the 3_0^1 band of HCN in which ν_3 is the C-H stretching vibration. The transition is of the $\Sigma^+ - \Sigma^+$ type showing clear P- and R-branch structure like a diatomic. However, unlike the diatomic case, there are two "hot bands" in which the low wavenumber vibration ν_2 is excited, overlapping the 3_0^1. One of these hot bands shows a P, Q and R branch centered around 3292 cm^{-1}, the other a P and R branch around 3290 cm^{-1}. Figure 9.8 (bottom) shows both the 3_0^1 transition (to the right), but also the 2_0^1 and 2_0^2 transitions at lower frequencies. In the 2_0^1 spectrum, the Q branch is clearly seen,

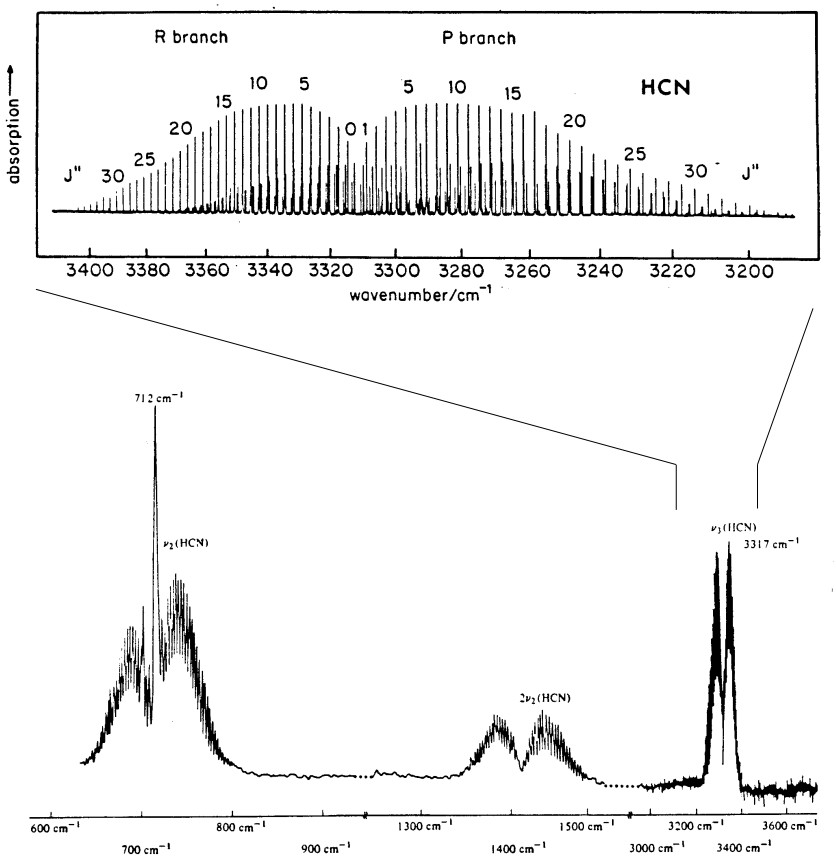

Figure 9.8– (Bottom) Portions of the infrared spectrum of HCN. The ν_2 bending vibration is of Π symmetry and therefore a perpendicular band with allowed P, Q, and R branches; while the ν_3 (C–H stretching) vibration has Σ symmetry and thus possesses only P and R branches. Note that the $2\nu_2$ overtone band is of $\Pi \otimes \Pi = \Sigma^+ \oplus \Delta$ symmetry, but only the Σ^+ component is allowed. (Top) Close up of the 3_0^1 C–H stretching vibration in HCN.

but in the overtone band 2_0^2 only P and R branches occur since the upper state has Σ^+ symmetry.

Figure 9.9 shows the rotational levels associated with a Π_u and a Σ_g^+ vibrational level, such as is the case for the 2_0^1 transition in CO_2. The Π_u set of rotational levels differs from the Σ_g^+ set of levels in two respects: (1) there is no J=0 level; and (2) each of the levels is split, with the splitting increasing with J. The reason for these differences is that the Π vibrational state has a quantum of "vibrational angular momentum" associated with it. To see how it arises in a degenerate vibration, look carefully at Figure 9.5.

Imagine that these two orthogonal components are equal in amplitude, but have a phase difference of $\pi/2$ radians. As a function of phase ϕ, nucleus X is 'up' at ϕ=0, 'into' the page at $\phi = \pi/2$, 'down' at $\phi = \pi$, and 'out' of the page at $\phi = 3\pi/2$, and similarly for the other nuclei. Thus, each nucleus can be thought of as describing a rotation about the internuclear axis. For non-degenerate vibrations, and for $v_i = 0$ in degenerate modes, this vibrational angular momentum $\overrightarrow{l}_i = 0$.

The angular momentum $\overrightarrow{l}_i$ also accounts for the splitting of the rotational levels,

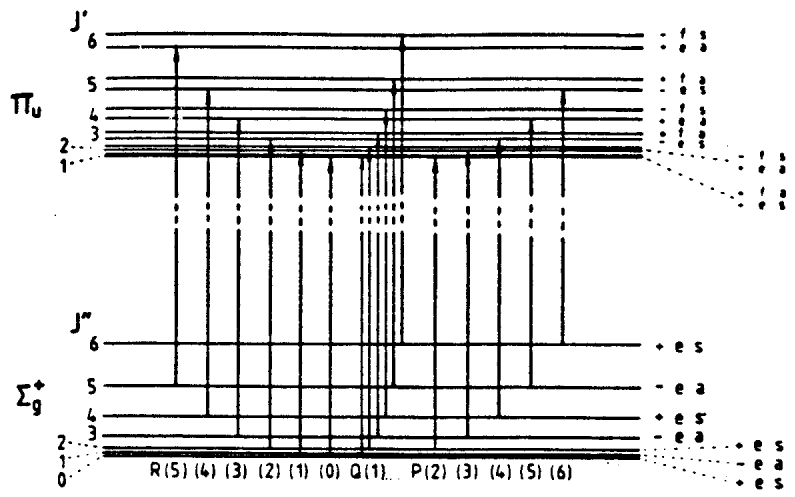

Figure 9.9– Rotational transitions in a $\Pi_u - \Sigma_g^+$ band.

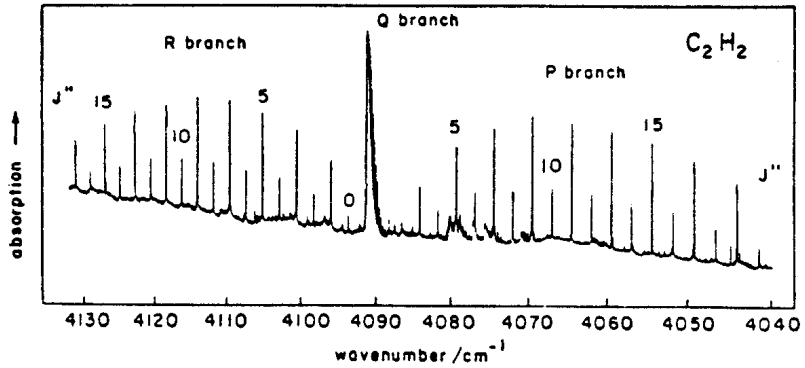

Figure 9.10– The $1_0^1 5_0^1$ Π_u – Σ^+ infrared band of acetylene.

resulting in "l-type doubling" of the levels with a splitting

$$\Delta\nu_i = q_i J(J+1). \tag{9.20}$$

This l-type doubling is similar to the Λ-type doubling discussed before.

Figure 9.10 shows another example of a $\Pi_u - \Sigma_g^+$ band for the case of acetylene, C_2H_2. The P, Q, and R branches are clearly seen. The 3:1 intensity alternation for J''=odd/even results from the fact that there are two equivalent protons, giving rise to *ortho-* and *para-* C_2H_2 (see § VIII.2c).

Another "perturbation" in spectra can arise when two vibrational modes interfere, because they lie very close in energy. A very famous example of such a "Fermi-resonance" is found for CO_2, where $\nu_1 \approx 2\nu_2$ (see Figure 9.11). The interaction between the two levels will shift the $2\nu_2$ level (0,2,0) down in energy, and the ν_1 level (1,0,0) up. Actually, only one of the two l-components, the $(0,2^0,0)$ component interacts with the (1,0,0) level, and the other l component $(0,2^2,0)$ remains unchanged in energy, where the quantum

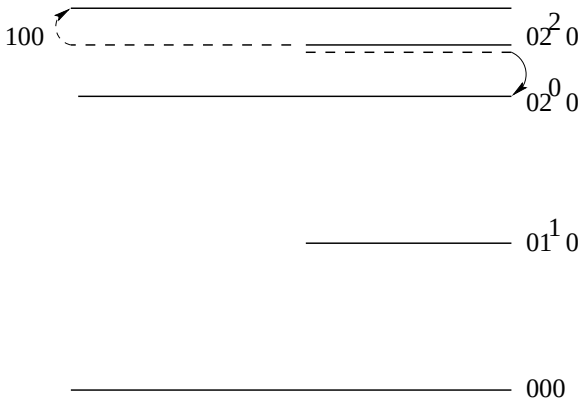

Figure 9.11– Fermi resonance in CO2. The broken lines go over to the solid lines indicated by the arrows under the influence of the Fermi resonance.

number l is added as a superscript to v_2 in the designation of the vibrational level. Such Fermi resonances are clearly observed in the spectra of CO_2 in, for example, the Earth's atmosphere (see Figure 9.12). Figure 9.13 shows part of the CO_2 bands observed in the spectrum of Mars.

(ii) Symmetric top molecules

The vibration-rotation spectra of a symmetric top molecule such as NH_3 can be analyzed in the same way as those of linear molecules. The normal modes of NH_3 are illustrated in Figure 9.14. The symmetry properties of the molecule allow certain of these modes to be infrared active.

Associated with each vibrational level are again the rotational levels for which the term energies are given by (8.30) or (8.31). Selection rules apply to the various rotational transitions. For more details, see for example, Herzberg Vol. II.

The infrared spectrun of NH_3 has been observed in planetary atmospheres such as that of Jupiter. It will be discussed in more detail in § IX.2d.

(iii) Spherical top molecules

Although a spherical rotor such as CH_4 has 9 normal modes, the vibrational selection rules for a molecule with such a high degree of symmetry become much more restrictive. The vibration-rotation spectrum of a spherical rotor looks quite similar to that of a $\Pi - \Sigma$ type of band in a linear molecule at low resolution.

Vibration-rotation bands of CH_4 have been detected in the atmospheres of all the outer giant planets, including Pluto, and in the atmosphere of Titan. They extend from about 7.7 μm in the infrared into the visible wavelength region. The prominent bands of methane that occur in the visible region, 6000-10000 Å, are inherently diffuse (see Figure 9.15). Attempts to assign them to individual overtones and combination tones show that the number of possible assignments can be in the thousands, each with a large number of individual lines. It is therefore plausible that they overlap completely, giving rise to a "diffuse spectrum". For such "quasi-continuum" spectra, the absorption obeys a simple exponential law, so that the bands can be used as an unambiguous measure of the CH_4 abundance. Since they absorb most of the red light, the planets will have a green-blue

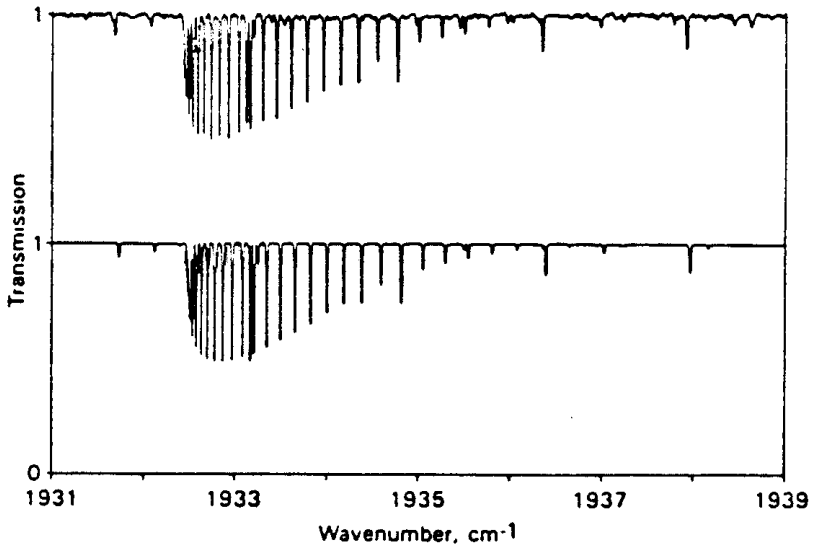

Figure 9.12– Observed and calculated lines in the Q-branch of the $3\nu_2$ band of CO_2 in the solar absorption spectrum. Spectral range, 1931 – 1939 cm^{-1}, tangent height 45.8 km. The upper panel presents the observed spectrum, that calculated from laboratory spectroscopy parameters and an atmospheric model is contained in the lower panel.

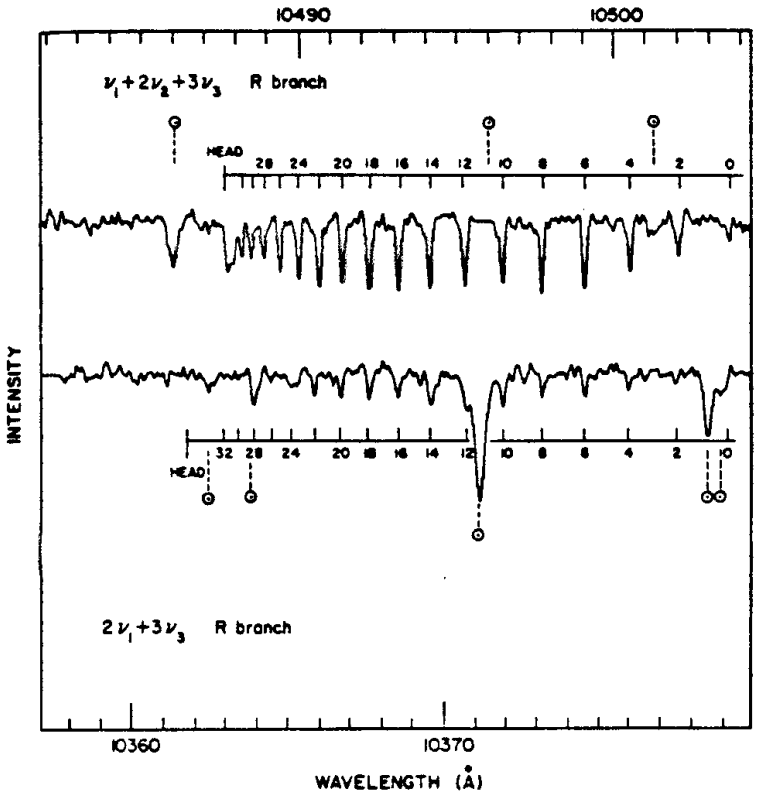

Figure 9.13– Two carbon dioxide bands in the spectrum of Mars. Solar lines are flagged.

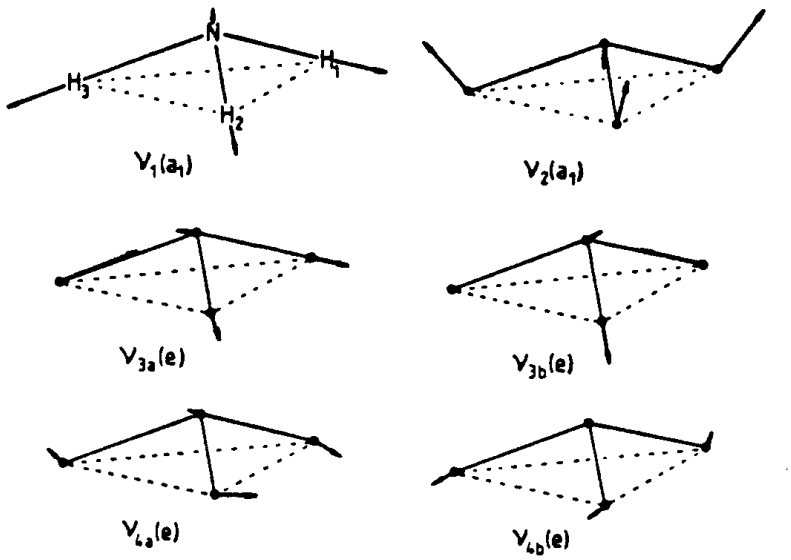

Figure 9.14– The normal modes of NH_3.

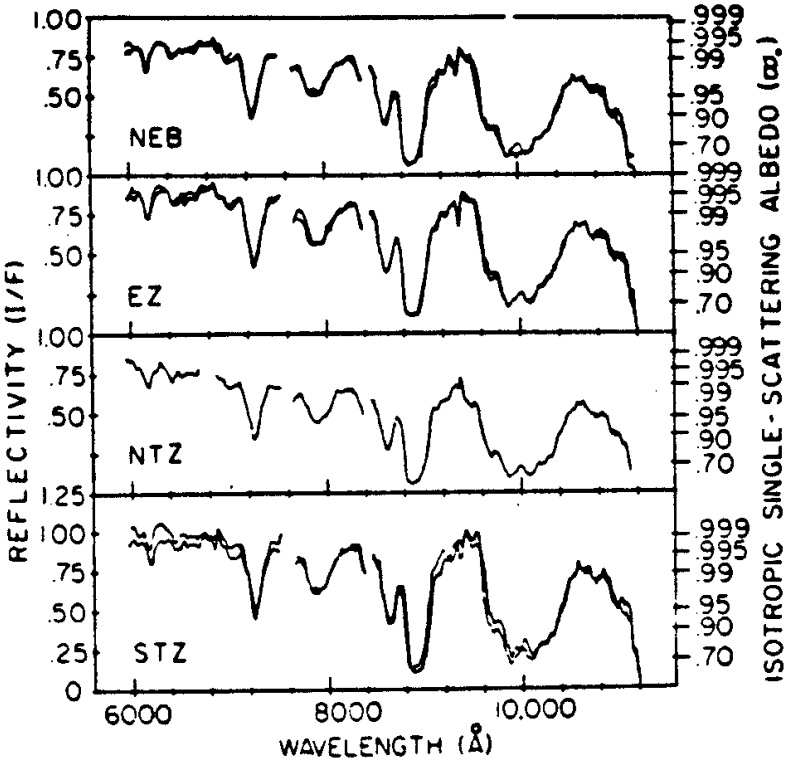

Figure 9.15– The reflectivities of four areas of Jupiter, showing the broad methane bands.

color, if the CH_4 abundance is high. The bands in the infrared, 3-7μm, behave in a more conventional way.

(iv) Asymmetric top molecules

As we have seen in § VIII.5, the rotational level structure of asymmetric top molecules is very complex, giving rise to very complex vibration-rotation bands. The rotational selectoin rules are also quite complex, but certainly include the usual requirement

$$\Delta J = 0, \pm 1$$

resulting in what may seem to be sets of randomly distributed P, Q, and R branches.

In an asymmetric top molecule like H_2CO (see Figure 8.4) the a, b and c principal inertial axes are defined by symmetry. It can be shown that the vibrational transition moments are confined to these a, b and c axes, giving rise to so-called type A, type B, or type C transitions. Each of these types of transitions has its own characteristic band shape. Some examples for the case of ethylene ($H_2C{=}CH_2$) are shown in Figures 9.16a-c. The type A band is dominated by a strong central minimum and moderately strong wings, and the type C band by a strong central peak and moderately strong wings. Thus, just a coarse glance at these spectra, even in cases that they are much less well-resolved, is usually sufficient to determine the symmetry of the vibration involved.

An example of an astrophysically important asymmetric top molecule is, of course, H_2O. Its vibration-rotation bands have been observed in the spectra of Mars, Venus, and Jupiter. In addition, water ice has been detected adsorbed on the surface of grains in interstellar clouds through infrared spectroscopy.

d) Anharmonicity

When anharmonicity effects are taken into account, the vibrational term values for a polyatomic molecule become

$$\sum_i G(v_i) = \sum_i \omega_i (v_i + d_i/2) + \sum_{i \le j} x_{ij} (v_i + d_i/2)(v_j + d_j/2) + \sum_{i \le j} g_{ij} l_i l_j + \ldots \qquad (9.21)$$

where x_{ij} are the anharmonic constants. For $i = j$, the x_{ij} are analogous to $-\omega_e x_e$ in a diatomic molecule, but for $i \neq j$ they involve combination vibrations, that is, coupling between different vibrations.

As for diatomics, the anharmonicity causes the vibrational levels to close up with increasing v. However, the anharmoncity can be quite different for the different normal modes. Consider as an example the CO_2 molecule, which has 3 normal vibrations, one of which is degenerate (see Figure 9.5). The potential energy surface V is thus 4-dimensional, and cannot be illustrated easily. However, by taking a section of the surface in two dimensions for each of the normal coordinates in turn, potential energy curves can be constructed for each of the coordinates.

Figure 9.17 illustrates a contour map of the potential energies V for the linear molecule CO_2. The coordinates on the axes are not the normal coordinates, but the two CO bond lengths $R_1 = R_2 = R_e$. Regions A_1 and A_2 are valleys lying higher in energy, since they correspond to removal of one oxygen atom, leading to O+CO. The "reaction coordinate" represents the pathway of minimum energy for the reaction from A_1 to B to A_2, and the variation of the energy along this coordinate is shown in the accompanying figure.

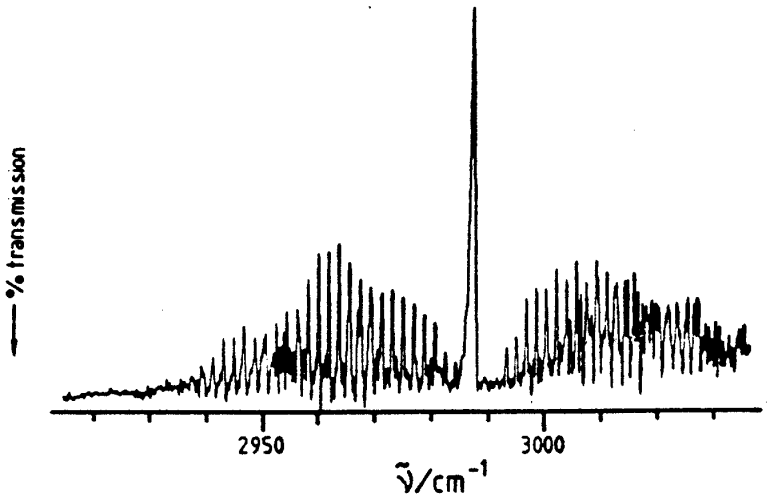

The 11^1_0 type *A* band of ethylene.

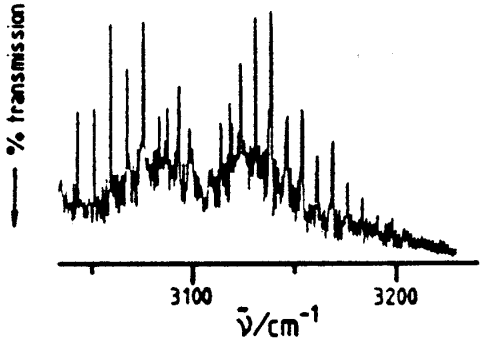

The 9^1_0 type *B* band of ethylene.

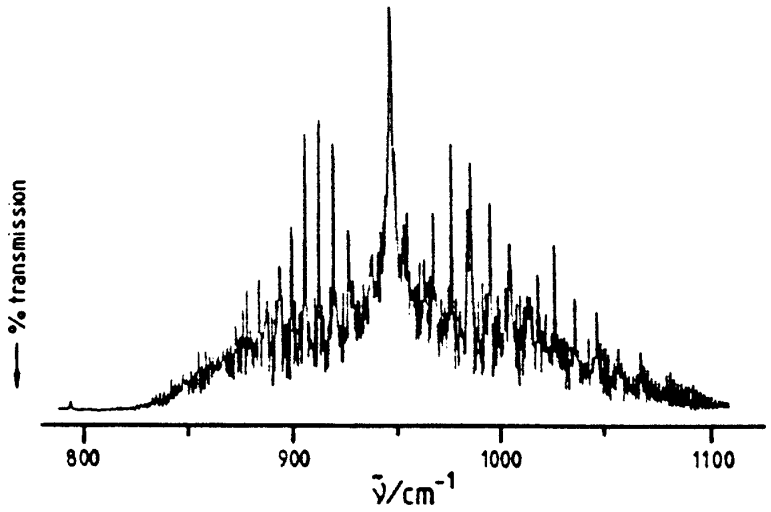

The 7^1_0 type *C* band of ethylene.

Figure 9.16– Spectra of C_2H_4 with A, B, and C type selection rules.

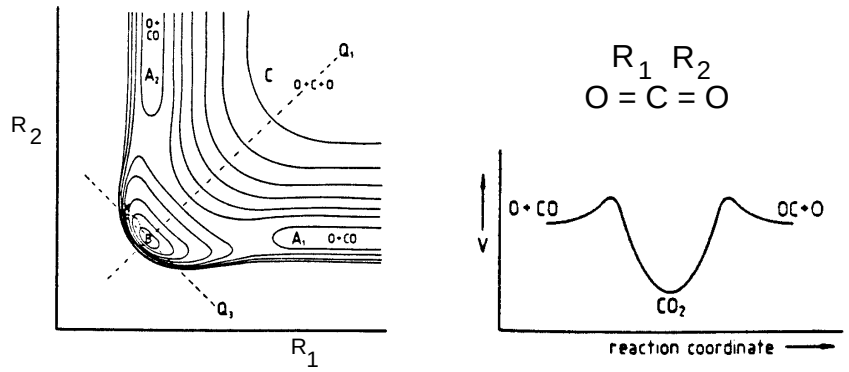

Figure 9.17– Contour of potential energy as a function of the two CO bonds.

In order to see how V varies with the two normal coordinates Q_1 and Q_3 corresponding to the symmetric and antisymmetric stretching vibrations ν_1 and ν_3 of CO_2, we have to determine how V varies along the dashed lines labelled Q_1 or Q_3. The resulting potential curves are shown in Figure 9.18. The one for ν_1 appears similar to that for a diatomic molecule, but the curve for ν_3 is symmetrical about the center. This example illustrates the important general point that for polyatomic molecules, some vibrations are "dissociative", such as ν_1, and others "non-dissociative", such as ν_3. The bending mode ν_2 is also non-dissociative and the corresponding potential curve is similar in shape to that for ν_3. For both potential curves in Figure 9.18, the vibrational levels are anharmonic, but in different ways, since the ν_1 levels converge to the dissociation limit, while those for ν_2 and ν_3 are more equally spaced and may actually show some divergence.

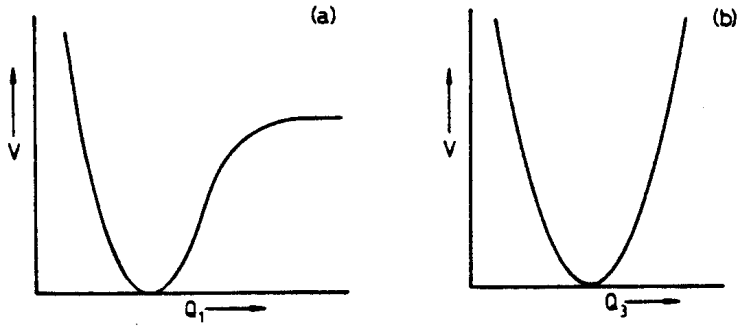

Figure 9.18– General shapes of the potential energy curves for the vibrations ν_1 (a) and ν_2 and ν_3 (b) of CO_2.

Another type of anharmonic potential is encountered, for example, for the NH_3 molecule. In the "inversion", or umbrella, vibration ν_2 of NH_3, the molecule goes through the planar configuration to an identical, but inverted, pyramidal configuration, as Figure 9.19 illustrates.

The pyramidal configurations (i) and (iii) obviously correspond to two identical minima in the potential energy, and the planar configuration (ii) to a maximum, resulting in a double minimum or W-shaped potential curve. The barrier height is the energy that would be required classically to go from the pyramidal to the planar configuration.

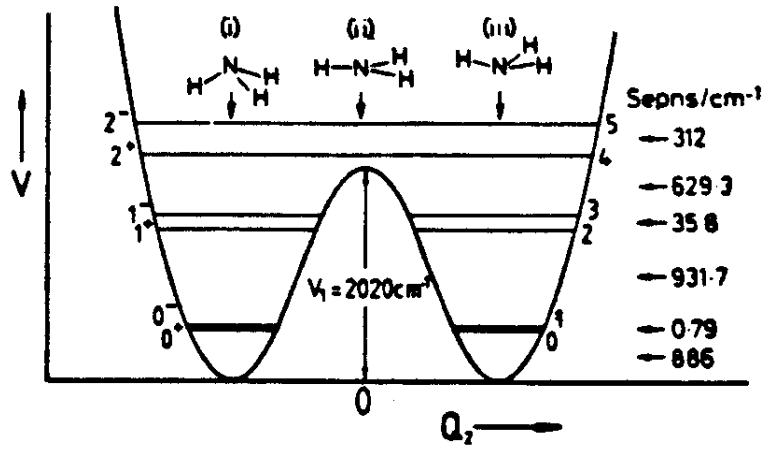

Figure 9.19– Potential energy curve for the inversion vibration ν_2 of HN_3.

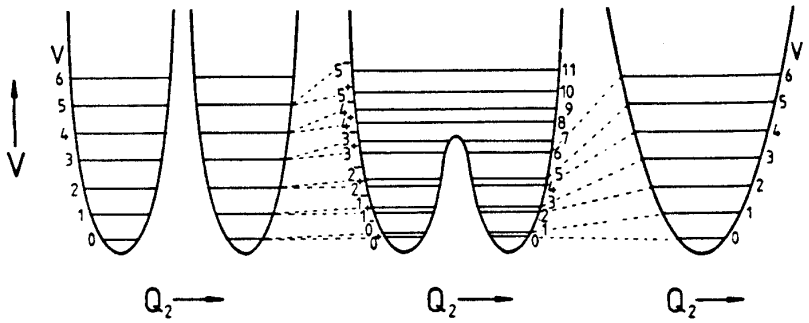

Figure 9.20– Potential energy curves and vibrational energy levels for an inversion vibration when the barrier to planarity is (a) infinite, (b) moderately low, and (c) zero.

However, quantum mechanically, the molecule can "tunnel" through the barrier, if it is not too high or too wide. In that case, an interaction occurs between the identical sets of vibrational levels in the two wells, splitting the levels into two components. This splitting becomes greater toward the top of the barrier where the tunneling is more effective, as Figure 9.19 shows. Figure 9.20 shows how the splittings and energy levels correlate as the barrier is decreased from infinitely high to zero.

The figure also illustrates that there are two alternative vibrational numbering schemes: 0, 1, 2, 3, ... in the zero barrier case, and 0^+, 0^-, 1^+, 1^-, ... relating to the high barrier case.

For NH_3, the splitting $\Delta\nu$ between the two levels is only 23.786 GHz for $\nu_2 = 0^- \leftrightarrow 0^+$, so that transitions between the levels occur in the microwave region. Indeed, the inversion splitting is significantly less than the splitting between the various rotational levels, so that effectively, each J_K level is split into two components. Figure 9.21 illustrates the level structure of NH_3. Inversion transitions of NH_3 have been observed both in interstellar clouds, and in the Jovian atmosphere.

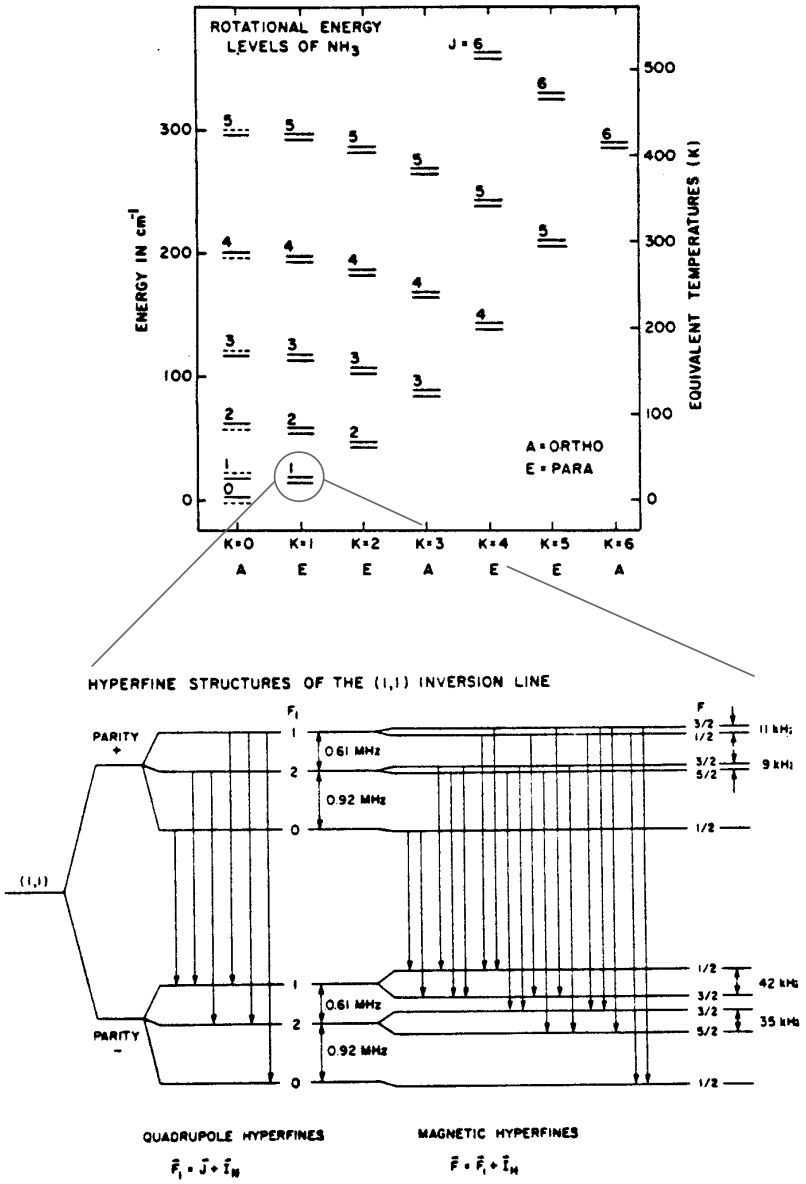

Figure 9.21– (Top) Energy level diagram of rotation-inversion states for ammonia. (Bottom) Nuclear hyperfine splittings in the $(J, K) = (1, 1)$ inversion transition of NH_3 (from Ho & Townes 1983, *Ann. Rev. Astr. Ap.* **21**, 239).

e) Small Molecule Examples

Various examples of vibration-rotation spectra in interstellar clouds, planetary atmospheres, and the atmosphere have already been shown. Figures 9.22-24 show some composite infrared spectra of Jupiter, some other planets, and of the Earth. An important aspect of the vibration-rotation spectra in the Earth's and planetary atmospheres is that they provide significant opacity, and prevent radiation from escaping. This can result in significant heating of the atmosphere, as in the case of CO_2 in the Earth's atmosphere. Measurements of the line shapes can be used to constrain the pressure or temperature structure in the atmosphere.

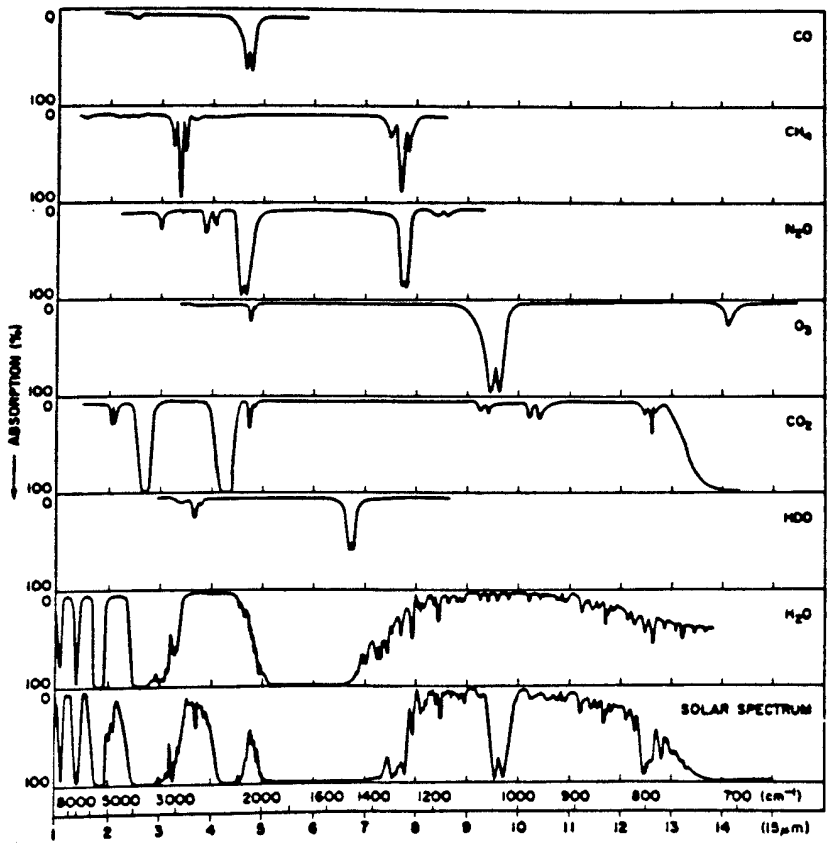

Figure 9.22– Low resolution spectrum of the Earth's atmosphere. The top six panels depict the absorption spectra of important atmospheric species, while the bottom panel is a simulated absorption spectrum of the atmosphere.

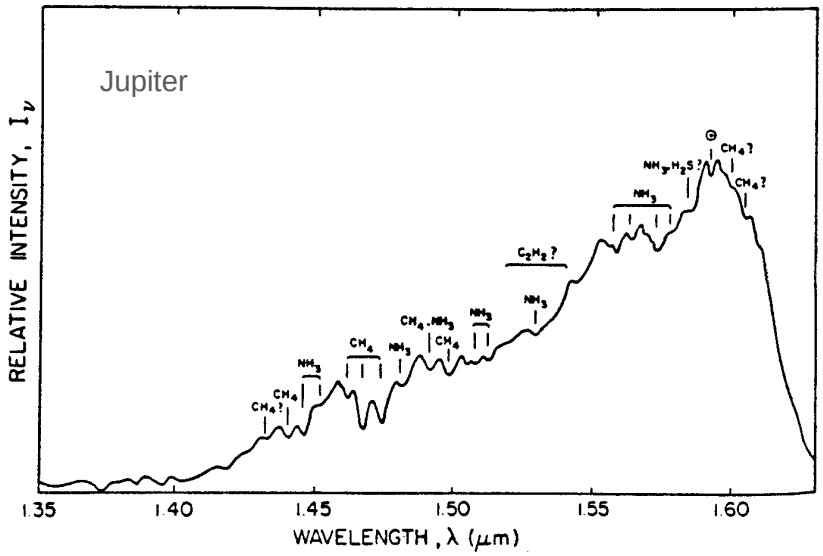

Figure 9.23– The 1.35-1.63 μm infrared spectrum of Jupiter, showing the many overtone and combination bands of ammonia and methane.

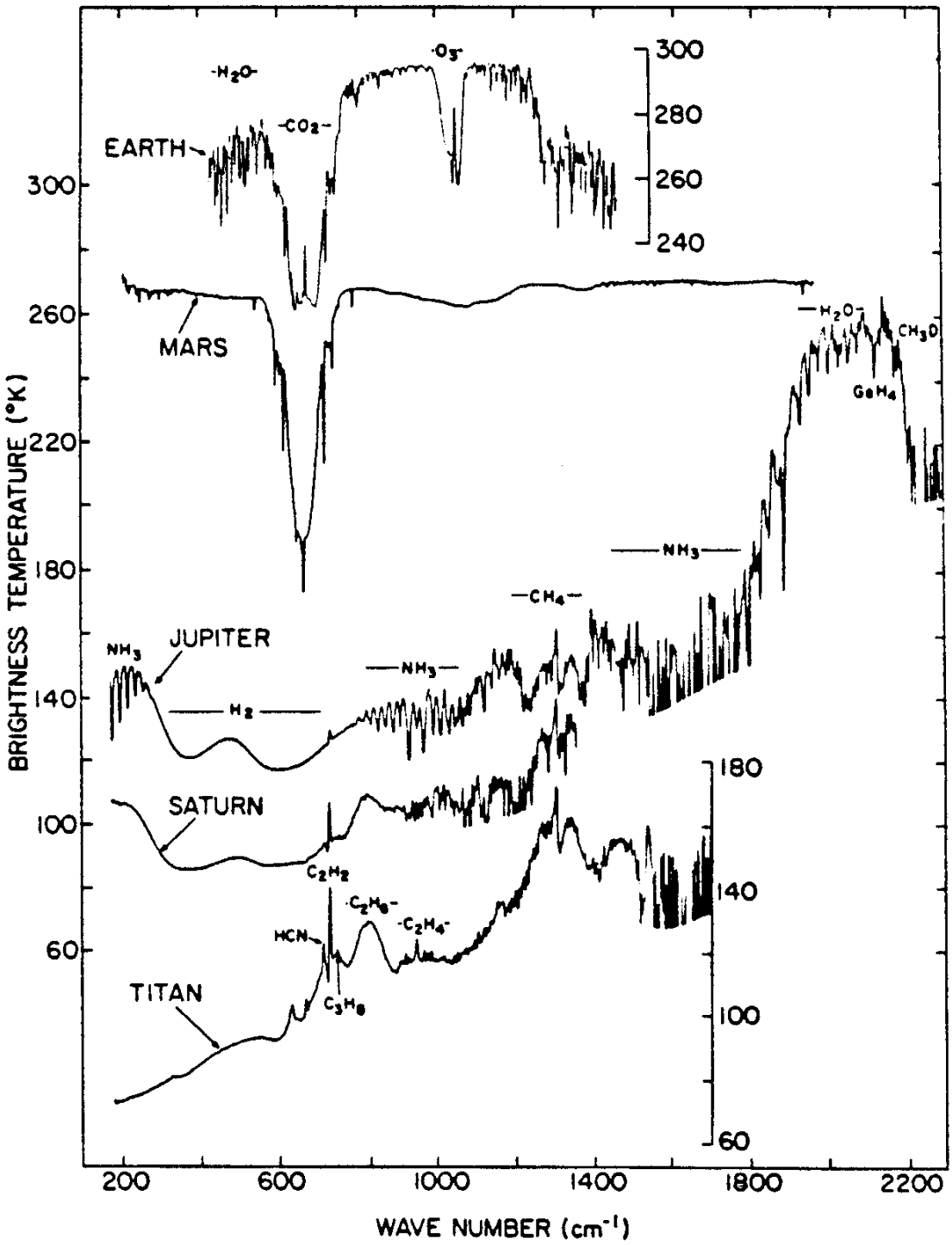

Figure 9.24– Planetary "thermal" infrared spectra for terrestrial and Jovian planets, plotted as brightness temperatures. Titan is included as well, being the only moon with a massive atmosphere. Features that are shown as "absorptions" are formed in a region of negative temperature gradients (typically the troposphere) while those that are in "emission" arise from a warmer stratosphere.

f) Characteristic Vibrational Frequencies of Functional Groups

Although in general, a normal mode of vibration involves movement of all atoms in a molecule, sometimes the movement is more or less localized in a part of the molecule. For example, if the vibration involves stretching or bending of a -X-Y group at the end of a molecule, where X is heavy compared with Y, the corresponding wavenumbers are almost independent of the rest of the molecule to which -X-Y is attached. From studying a wide range of organic molecules, it has been found, for example, that most ketones and other molecules containing the C=O group have a strong vibrational feature near 1715-1735 cm^{-1} which is assigned to a C$\Longleftrightarrow$O stretching vibration. Similarly, C$\longleftrightarrow$C single bond vibrations are found to occur in the 800-1200 cm^{-1}, or "fingerprint" region, with the exact frequencies and patterns of vibrations dependent on the the structure of the molecule. Conversely, in ethyl alcohol (CH_3CH_2OH), which is an abundant interstellar molecule, the motions of the -OH group are approximately those which it would have if it were attached to an infinite mass by a bond with force constants typical of an OH bond. Thus, one can assign a typical wavenumber range to an OH-stretching vibration of 3590-3650cm^{-1} in the absence of hydrogen bonding. Such a typical wavenumber is called a "group wavenumber". Another example of the OH group is the bending vibration, which typically 1050-1200 cm^{-1}, nearly independent of the exact nature of the molecule it is attached to. Also, the force constants in, for example, C-C, C=C, C$\equiv$C bands are quite dissimilar, so that their stretching can be considered independent, even if they occur in a molecule like HC$\equiv$C–CH=CH_2.

At first site, the existence of characteristic group frequencies may seem hard to reconcile with the normal mode approach in which most or all of the atoms vibrate at specific frequencies in a collective fashion. Recall that for certain vibrations (the symmetric stretch in CO_2, for example) the vibrational amplitudes of certain atoms in the molecule are very small or zero, and the vibrations can therefore be considered to be localized to some extent. The wide range of spectra now obtained for organic species (well in excess of 100,000 at this point!) reveal consistent wavelengths for different functional groups, which means the force constants involved are, in some sense, characteristic.

Let's think about X–H stretches as an example, where X = C,N,O. In the pseudo-diatomic limit, the reduced mass reduces to $\mu \sim m_{\rm H}$, and the vibrational frequency then simply becomes

$$\nu({\rm X-H\ str}) \approx \frac{1}{2\pi}\left[\frac{k({\rm X-H\ str})}{m_{\rm H}}\right]^{1/2} \quad . \tag{9.22}$$

The typical frequency for an O–H stretch is roughly 3600 cm^{-1}, which corresponds to a force constant of $k({\rm O-H\ str})$=7.6 $\times$ 10^5 dynes/cm. Similar considerations apply to N–H and C–H stretches, both of which occur in the 3000 cm^{-1} region. These frequencies are rather high compared to other modes in the molecule, and so it is perhaps not surprising (given the discussion of Lecture #16) that these modes can be treated separately.

What about modes like the C=O stretch, however, which lie rather close to any number of other modes in a large organic molecule? What it basically comes down to are the force constants, as first outlined by Bartholomé and Teller in the 1930s. From a classical analysis of coupled springs, it is found that if the force constant of a given pair of oscillators is very different than that of the other force constants in the system, the vibrational frequency is

only slightly altered from what it would be in a purely diatomic model of the vibration with the same force constant. For the C=O vibration, the nearly modes tend to involve single bonds, which have much smaller force constants than does the carbonyl group. Similar behavior is found when the reduced masses are quite different, and so vibrations involving the halogens (Cl, Br) also tend to behave "independently." When both the force constants and masses are similar, the skeletal vibrations of a molecule interact strongly and are spread over a wide frequency range. For organic molecules this occurs primarily near 10 μm, hence its labeling as the fingerprint region.

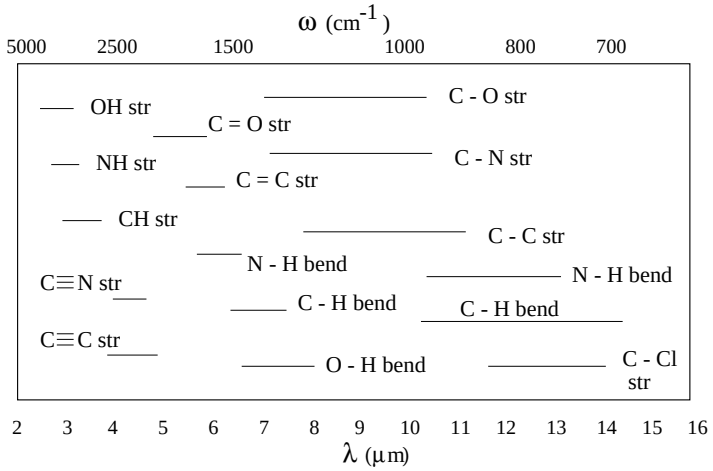

Figure 9.25 – A simplified overview of the characteristic vibration frequencies of common organic functional groups.

Typical group vibrational wavenumbers for bond-stretching and angle-bending vibrations are given in Table 9.2 and summarized graphically in Figure 9.25. Note, however, that not all vibrations are group vibrations. Some normal modes involve strong coupling between stretching or bending motions of atoms, and are called "skeletal vibrations". These tend to be highly specific to a particular molecule, and occur typically in the 300-1300 cm^{-1} range. This spectral region is therefore sometimes called the "fingerprint region", whereas the 1500-3700 cm^{-1} range, where many group vibrations occur, is the "functional group" region of the spectrum.

In the figures that follow, IR spectra for a number of compounds are presented that illustrate the common features observed in organic molecules. Below we briefly summarize how to look at such spectra to glean the kinds of structural information that can be extracted from them. There exist several excellent textbooks which consider the role of IR spectroscopy in organic analyses in detail, should you be interested in learning more about this subject. A good one is "Introduction to Spectroscopy" by D.L. Pavia, G.M. Lampman, and G.S. Kriz (W.B. Saunders Co., Philadelphia, 1979), which covers not only IR spectroscopy but NMR, UV/Vis, and mass spectrometric methods.

In trying to understand the spectrum of some unknown (or known) compound, it is best to first try and determine whether certain major functional groups are present or not. Peaks from C=O, O-H, N-H, C-O, C=C, C≡C, C≡N, and NO_2 groups are often the most conspicuous and provide immediate structural information when they are present. It can be difficult to extract detailed information from the C-H stretching absorptions near 3000

Table 9.2 – A Simplified Correlation Chart for IR Spectra

Group	Vibration	Frequncy (cm^{-1})	Wavelength (μm)	Intensity
C–H	Alkanes (stretch)	3000-2850	3.33-3.51	s
	-CH_3 (bend)	1450, 1375	6.90, 7.27	m
	-CH_2- (bend)	1465	6.83	m
	Alkenes (stretch)	3100-3000	3.23-3.33	m
	(out-of-plane bend)	1000-650	10.0-15.3	s
	Aromatics (stretch)	3150-3050	3.17-3.28	s
	(out-of-plane bend)	900-690	11.1-14.5	s
	Alkynes (stretch)	ca. 3300	ca. 3.03	s
	Aldehydes	2900-2800	3.45-3.57	w
		2800-2700	3.57-3.70	w
C–C	Alkanes	1400-700	∼7-14	m-w
C=C	Alkene	1680-1600	5.96-6.25	m-w
	Aromatic	1600, 1475	6.25, 6.78	m-w
C≡C	Alkyne	2250-2100	4.44-4.76	m-w
C=O	Aldeyhyde	1740-1720	5.75-5.81	s
C=O	Ketone	1725-1705	5.80-5.87	s
C=O	Carboxylic acid	1725-1700	5.80-5.88	s
C=O	Ester	1750-1730	5.71-5.78	s
C=O	Amide	1670-1640	6.00-6.10	s
C=O	Anhydride	1810, 1760	5.52, 5.68	s
C=O	Acid Chloride	1800	5.56	s
C-O	Alcoholes, ethers, esters	1300-1000	7.69-10.0	s
	Carboxylic acids, anhydrides			
O–H	Alcohols, Phenols			
	Free	3650-3600	2.74-2.78	m
	H-Bonded	3500-3200	2.86-3.13	m
	Carboxylic acids	3400-2400	2.94-4.17	m
N–H	Prim. & Sec. Amines,	3500-3100	2.86-3.23	m
	amides (stretch)			
	(bend)	1640-1550	6.10-6.45	m-s
C–N	Amines	1350-1000	7.4-10.0	m-s
C=N	Imines & Oximes	1690-1640	5.92-6.10	w-s
C≡N	Nitriles	2260-2240	4.42-4.46	m
X=C=Y	Allenes, Ketenes, Isocyanates	2270-1950	4.40-5.13	m-s
	Isothiocyanates			
N=O	Ntrio (R-NO_2)	1550, 1350	6.45, 7.40	s
S-H	Mercaptans	2550	3.92	w
S=O	Sufoxides	1050	9.52	s
	Sulfones, Sulfonyl Chlorides	1375-1300 &	7.27-7.69	s
	Sulfates, Sulfonamides	1200-1140	8.33-8.77	s
C–X	Fluoride	1400-1000	7.14-10.0	s
	Chloride	800-600	12.5-16.7	s
	Bromide, Iodide	<667	>15.0	s

cm^{-1} since almost all compounds have these features. Below we present a major check list of the important overall features:

1. Is a carbonyl group present?

   The C=O group gives rise to a strong absorption feature in the 1820-1660 cm^{-1} region (λ=5.5-6.1 μm). This peak is often the strongest in the spectrum and is of medium width. You can't miss it! An example is provided by the benzoic acid spectrum presented in Figure 9.26.

2. If C=O is present, check for the following types (if absent, go to 3.):

   ACIDS. Is OH also present? This will give rise to *broad* absorption near 3400-2400 cm^{-1} (which usually overlaps with the C–H stretching bands). This is shown in the benzoic acid spectrum in Figure 9.26 and also in the acetylsalicylic acid (aspirin) spectrum in Figure 9.27.

   AMIDES. Is NH also present? Here you'll find medium absorption near 3500 cm^{-1} (2.85 μm), which is sometimes split into a doublet.

   ESTERS. Is C–O also present? These will be manifest as strong absorptions near 1300-1000 cm^{-1} (c.f. Figure 9.27).

   ANHYDRIDES. These have *two* C=O features near 1300-1000 cm^{-1} (7.7-10.0 μm).

   ALDEHYDES. Is the aldehyde C–H stretch present? These are the longest wavelength C–H stretching features near 2850 and 2750 cm^{-1}.

   KETONES. The above five choices have been eliminated.

3. If C=O is absent, check for:

   ALCHOHOLS, PHENOLS. Check for O–H, which gives broad absorptions over 3600-3300 cm^{-1} *and* C–O stretches near 1300-1000 cm^{-1}. Note that the hydrogen bonded broadening is not as great as for carboxylic acids. This is illustrated by the α-napthol IR spectrum presented in Figure 9.28.

   AMINES. Look for N–H via medium absorptions near 3500 cm^{-1}, or 2.85 μm. As an example, we present the IR spectrum of aniline in Figure 9.29.

   ETHERS. Check for the presence of C–O near 1300-1000 cm^{-1}, and the absence of O–H.

4. Double bonds and/or aromatic rings.

   By itself, a C=C double bond produces a *weak* absorption feature near 1650-1450 cm^{-1}. A series of absorptions in the 6-7 μ range often imply an aromatic ring. This can be checked by consulting the C–H stretch region; aromatic and vinyl CH stretches occur to the left of 3000 cm^{-1} (to higher frequency). The aliphatic versus aromatic C–H stretch differences are illustrated in Figures 9.30 and 9.31 (*p*-di-*t*-butylbenzene and fluorene, respectively). For multi-ring aromatic systems, the C=C stretching features move to longer wavelengths, and there are often strong features longward of 12-13 μm associated with the out-of-plane bending vibrations of the system.

5. Triple Bonds.

   C≡N is a sharp, medium absorption near 2250 cm−1, C≡C is a weak but sharp absorption near 2150 cm−1. The latter can also be checked for with the acetylenic CH stretch near 3300 cm^{-1} (for terminal C≡C groups).

6. Nitro Groups.

   The R-NO_2 topology is characterized by *two* strong absorptions at 1600-1500 and 1390-1300 cm^{-1}.

7. Halogen Atoms.

   The presence of F, Cl, and Br is manifest as *strong* features longward of 8-10 μm, as the spectrum of *para*-toluene in Figure 9.32 illustrates. These features are important in global warming since the earth's atmosphere is relatively transparent from 7.5-13 μm, and the C–F and C–Cl stretches in freons provide one of the few strongly absorbing chromophores (apart from silicates) in this spectral region.

8. Hydrocarbons (non-aromatic).

   If none of the above features are found, you're probably dealing with a hydrocarbon. The major absorptions lie in the C–H stretch region near 3000 cm^{-1}, and the spectrum will otherwise be relatively simple – at least for purely aliphatic systems where the only additional feature of note occur between 1450 and 1375 cm−1.

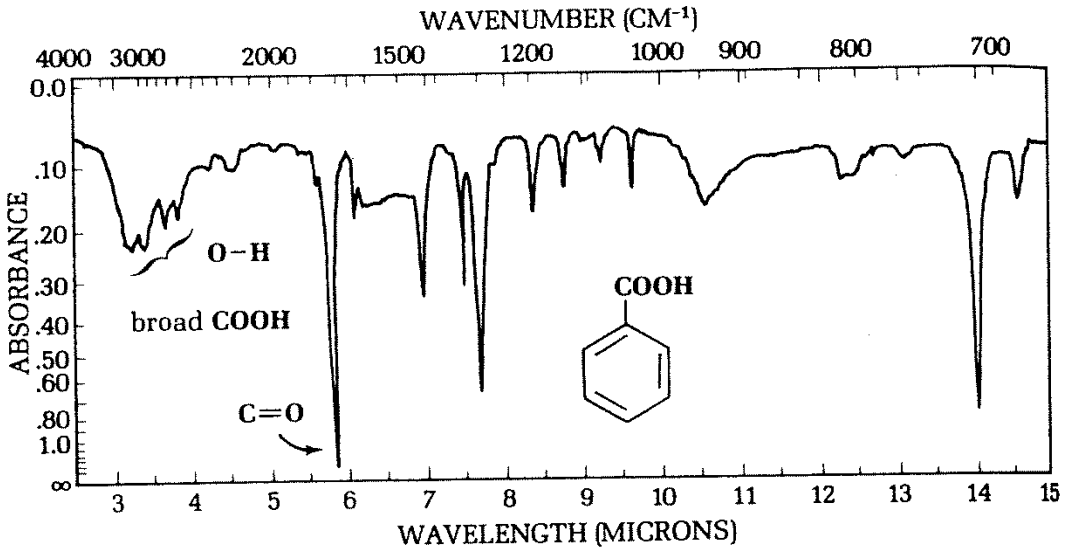

Figure 9.26– The infrared spectrum of benzoic acid (in CS_2). Note the strong C=O stretch and very broad O–H stretching vibrations characteristic of carboxylic acid groups.

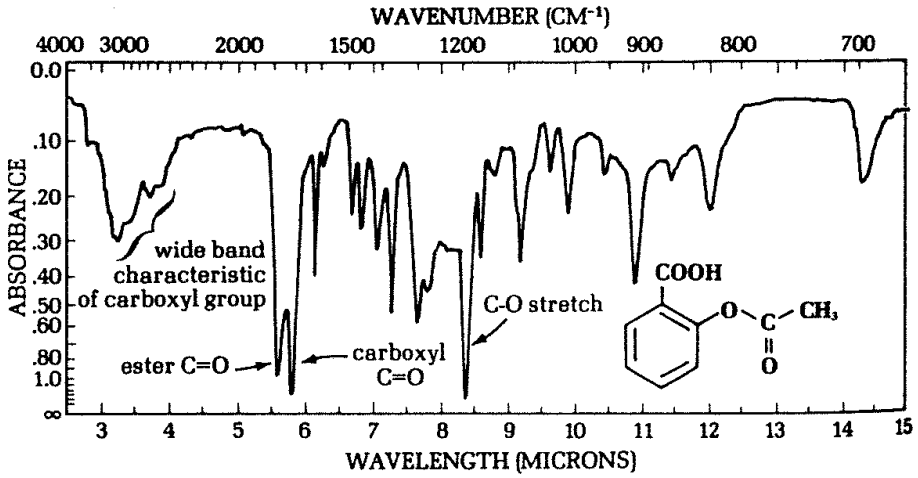

Figure 9.27– The infrared spectrum of acetylsalicylic acid (aspirin, in $CHCl_3$). Note that in addition to the the strong C=O stretch and very broad O–H stretching vibrations characteristic of carboxylic acid groups, there is a noticeable splitting between the carboxylic acid and ester C=O vibration, and an additional strong feature at longer wavelengths due to the C–O stretch.

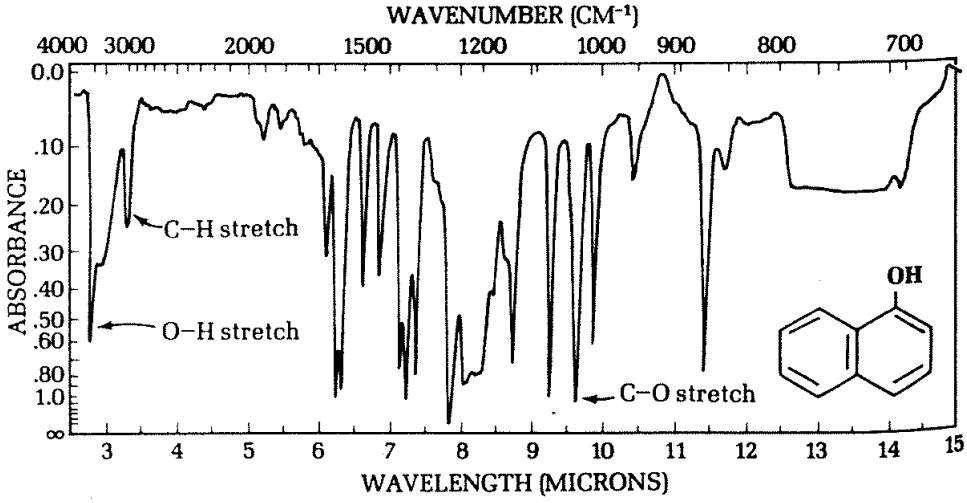

Figure 9.28– The infrared spectrum of α-napthol. Here, the hydrogen bonded leads to a broadening of the O–H stretch, but not nearly as much as for the carboxylic acid interaction (the C–H stretch is now visible). The C–O stretch is now buried amongst the considerable vibrational feature density of the aromatic rings.

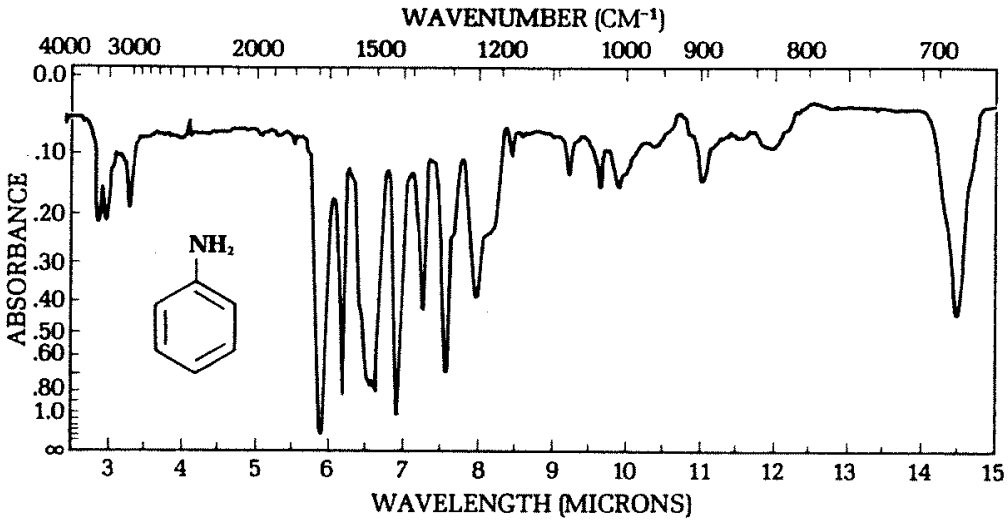

Figure 9.29– The infrared spectrum of aniline. Note the greatly reduced hydrogen bonded capability of the amino group, and the lack of a strong C–N counterpart to the C–0 stretch.

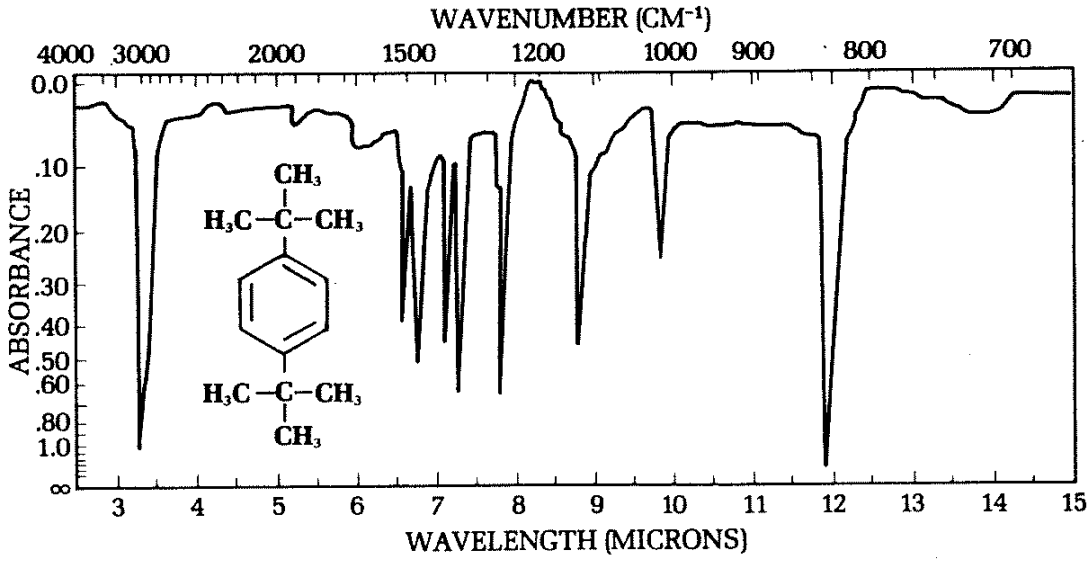

Figure 9.30– The infrared spectrum of *para*-di-*tert*-butylbenzene. Among the strongest features are now the C–H stretch. This is a clue that the molecule likely does not contain heteroatoms. The large number of features in the 6-9 μm range are mostly aromatic ring vibrations.

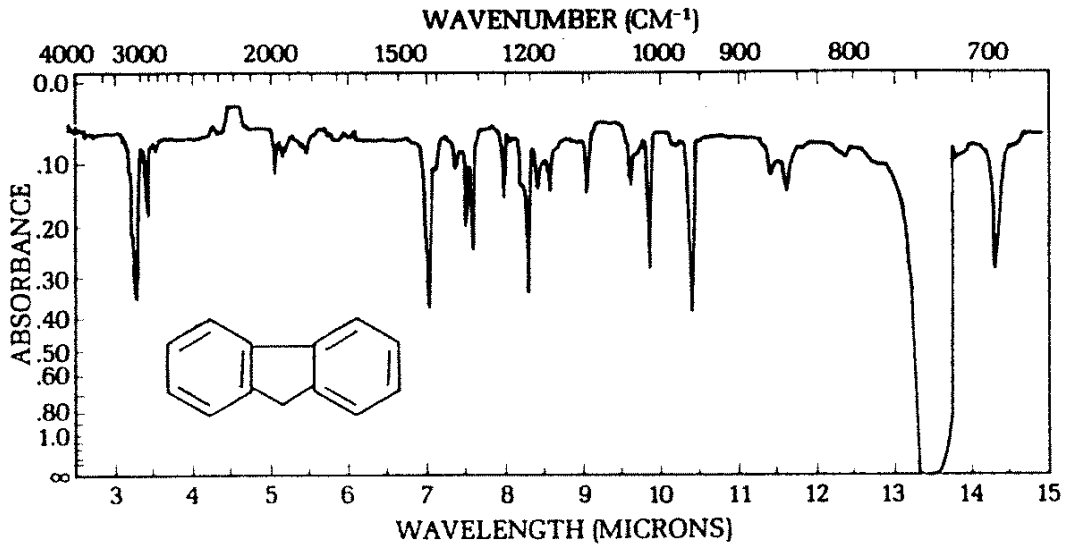

Figure 9.31– The infrared spectrum of fluorene. As is true in Figure 17.6, the C–H stretches are among the strongest features. Here they have moved a bit to the blue, a clue that the hydbridization is sp^2 and not sp^3. The extensive vibrational patterns near 6-8 μm also are indicative of aromaticity, while the strong feature longward of 12 μm arises from the out-of-plane bend, and let's you know the molecule has at least two rings.

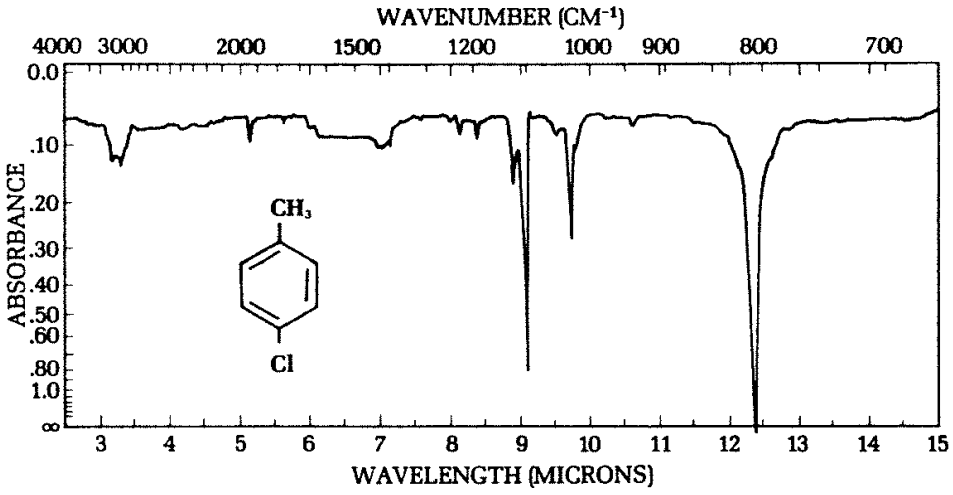

Figure 9.32– As is true for many Cl- or F-containing compounds, by far the strongest feature is the C–Cl stretch beyond 10 μm.

f) Solid State Materials/Large Molecule Examples

Silicates and Icy Grain Mantles in Absorption

The spectra on the preceeding pages were acquired as either neat liquids or pressed solid pellets; and point out a significant advantage of vibrational over rotational spectroscopy – molecules in either the gas or condensed phase give rise to vibrational spectra. Further, as Figure 9.33 shows, important molecules without dipole moments (e.g. CO_2) are available for study. For a gas of solar composition, summing up all the condensible mass yields a total of about 1% of the mass contained in hydrogen and helium. While some of this mass, particularly among the volatile elements C, N, and O, resides in the gas phase, much of it is present as $\lesssim \mu$m-sized dust grains. How do we know this?

The dust grains are excellent scatterers of UV and optical radiation, and by measuring the amount of extinction along given lines of sight as a function of wavelength, it is possible to constrain the size distribution of the dust. Spectroscopy of various vibrational features then leads to an assessment of the *composition* of the dust. Two major classes of grains are found, silicates and carbonaceous grains. Silicates are based principally on silicon atoms that are surround by tetrahedral arrangement of oxygen atoms. This unit gives rise to two intense peaks near 10 and 18 μm that vary only slightly with composition. Thus, nearly all silicates have bands here and so intense absorption features are seen toward lines-of-sight with strong IR background sources (c.f. Figure 9.33). We'll look at the carbonaceous grains after we learn a bit more about the silicates.

In the dense gas that forms stars, the gas becomes sufficiently cold that *icy mantles* accrete onto the grain surfaces. The other bands visible in Figure 9.33 arise from such an icy coating, and is dominated in most objects by water ice, which has a strong, broad absorption near 3 μm. Other molecules of note include CO, CO_2, and CH_3OH. We'll make a comparison of grain mantle chemistry and cometary chemistry later in the class.

Here's, let's concentrate on what these sort of spectra tell us. Figures 9.34 and 9.35 present close up views of the CO stretching band near 4.7 μm and the CO_2 bending vibration near 15.2 μm. The high resolution CO spectrum nicely illustrates the difference between gas phase and solid state spectra. When gas phase molecules are seen in absorption such as in Figure 9.34, the standard curve-of-growth techniques outlined earlier for atoms can be used to calculate the column densities once the oscillator strengths are known. For vibrational spectroscopy, the best such database is called HITRAN (for HIgh resolution TRANsmission spectrum of the Earth's atmosphere), though not all important interstellar molecules are included. You'll be introduced to the mechanics of HITRAN and its use in column density calculations in the final problem set.

Going back to the icy mantles, Instead of a suite of rovibrational lines, the solid state spectrum consists of a smooth band. The *shapes* of these bands are related to the *environments* in which the host molecules find themselves. In Figure 9.34, the broad absorption feature between 2122-2149 cm^{-1} can be entirely attributed to the stretching vibration mode of ^{12}CO in interstellar (or circumstellar) ices. The high spectral resolution achieved allows the unambiguous separation of gas phase and solid state CO, and a detailed study of the solid CO band profile. From these and other spectra, CO is found to exist in both polar (i.e. water-dominated) and apolor (that is, CO, N_2 or CO_2-dominated ices) environments along the same line-of-sight. From laboratory studies of such ices,

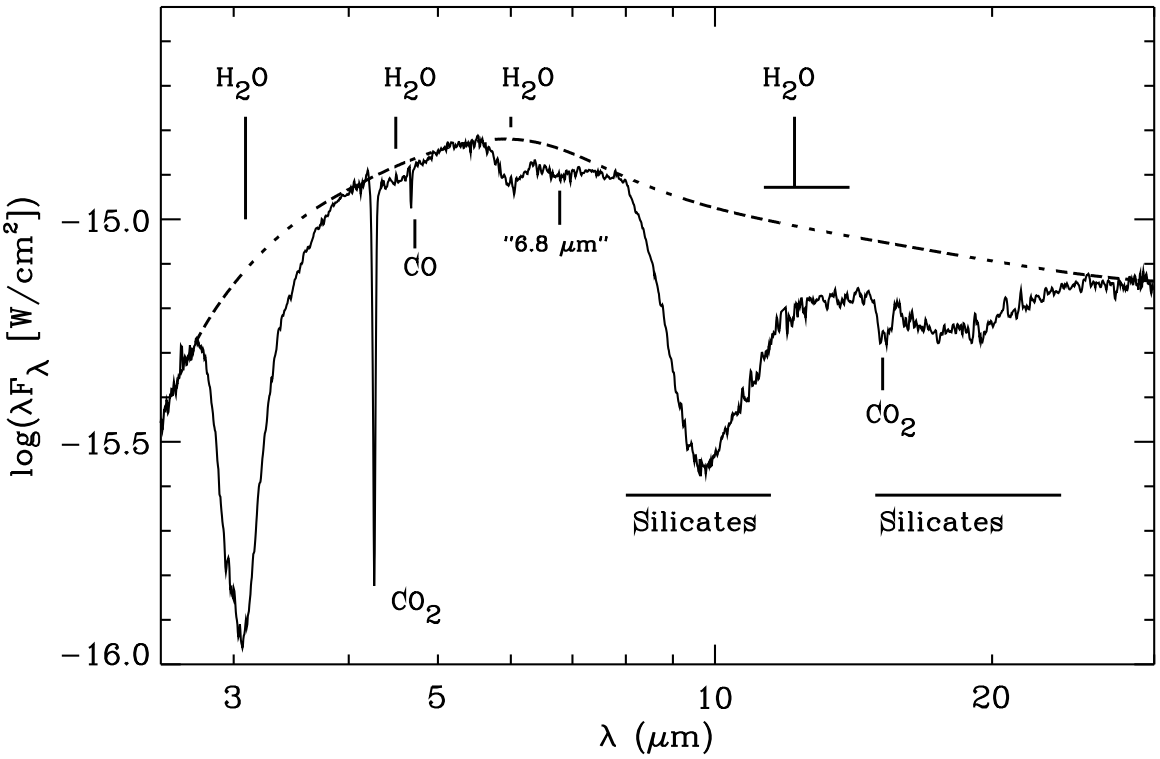

Figure 9.33- The mid-infrared spectrum of the protostar Elias 29 acquired by the Short Wavelength Spectrometer aboard the Infrared Space Observatory (ISO-SWS).

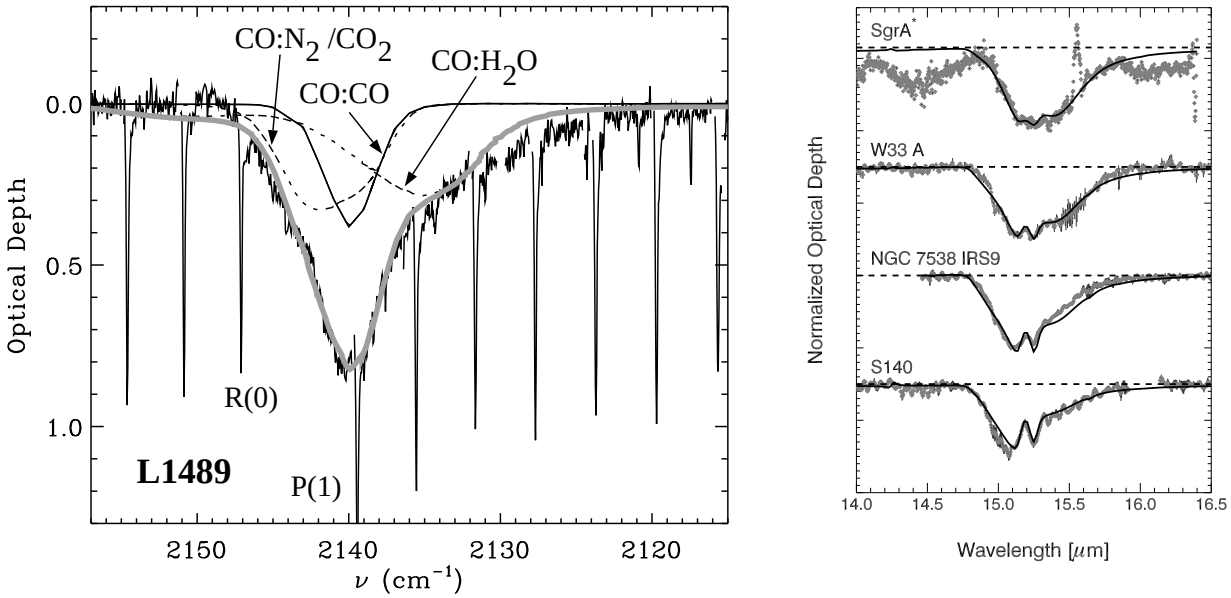

Figure 9.34- (Left) The Keck NIRSPEC $\lambda/\Delta\lambda \approx 25,000$ CO spectrum of the protostar L1489. **Figure 9.35**– (Right) ISO-SWS CO_2 ice bending mode spectra toward a number of high mass protostars. Temperature increases toward the bottom.

the fits to the spectrum in Figure 9.34 yield three components to the spectrum: a polar H_2O:CO=4:1 ice (T=50 K; dotted) to account for the long wavelength wing, an apolar N_2:O_2:CO_2:CO=1:5:0.5:1 ice (T=10 K; dashed) for the short wavelength wing, and a pure CO ice ('CDE' shape; T=10 K; solid) that fits the central peak. The particle shape is also important in fitting these profiles, and the thick solid line is the sum of the three laboratory components with the best estimate of particle shape effects.

Finally, the solid CO column density can derived by dividing the integrated optical depth over the so-called band strength A. For solid CO, laboratory measurements have determined $A = 1.1 \times 10^{-17}$ cm molecule^{-1} independent of ice composition. For the spectrum in Figure 9.34, this yields N(solid CO)=6.5×10^{17} cm^{-2}. CO in polar ices contributes N=3.5×10^{17} cm^{-2} to the total column, the apolar components at 2140 and 2142 cm^{-1} contribute about equally, or N=1.5×10^{17} cm^{-2} for each. A curve-of-growth analysis yields a gas phase CO column density of $\sim 6 \times 10^{18}$ cm^{-2}, and so the CO ice/CO gas ratio is about 0.1 in this source.

Similar analyses can be performed for other species such as CO_2, which forms the basis of Figure 9.35. Here, the interesting sub-structure in the CO_2 band profile is caused by an intermolecular interaction with methanol molecules in the ice. The sources in Figure 9.35 are displayed in order of increasing gas phase temperatures in the material around the young star, as measured by either millimeter-wave emission lines from molecules such as CO or HCN, or the rotational temperature found via absorption spectroscopy of gas phase water (in the near-infrared). The solid lines present fits based on laboratory spectroscopy of H_2:CH_3OH:CO_2=1:1:1 at temperatures ranging from 106 - 118 K (which, due to background pressure differences, corresponds to 50 - 60 K under interstellar conditions).

Silicate Emission from Circumstellar Disks

Clearly, the ices vary considerably. What about the refractory grains themselves? Over the past decade, an evolutionary model of star formation has arisen based, in part, on their spectral energy distributions, or SEDs. Very young stars are surrounded by large amounts of cold material, while those that have accreted most of their mass have only tenuous envelopes of much warmer gas and dust. ISO presented the first opportunity to examine these SEDs at high spectral resolution and without the interference of the Earth's atmosphere. As Figure 9.36 illustrates, this evolutionary sequence is well illustrated by clear, yet sometimes subtle, changes in their SEDs. Young objects are dominated by solid-state absorption features (principally ices and amorphous silicates) due to the large column of cold gas and dust between the young star and the observer. In older objects, the star becomes optically visible and its intense radiation field from the IR to the UV begins to drive the production of gas phase emission lines and *emission* features from carbonaceous grains (the "PAHs" in Figure 9.36, more below) and silicates.

These emission fetures are produced by the interaction of stellar and interstellar radiation with the surfaces of the accretion disks surrounding young stars. A warm surface layer is produced that surrounds a colder interior if the accretion disk is optically thick. Hence, optical and infrared observations are tracing only a small fraction of the mass of the disk. Interestingly, in the older disk sources and in solar system planetesimals such as comets and carbonaceous chondrites, *crystalline* silicate features are observed. These latter changes may be related to processes of grain coagulation, settling, and destruction

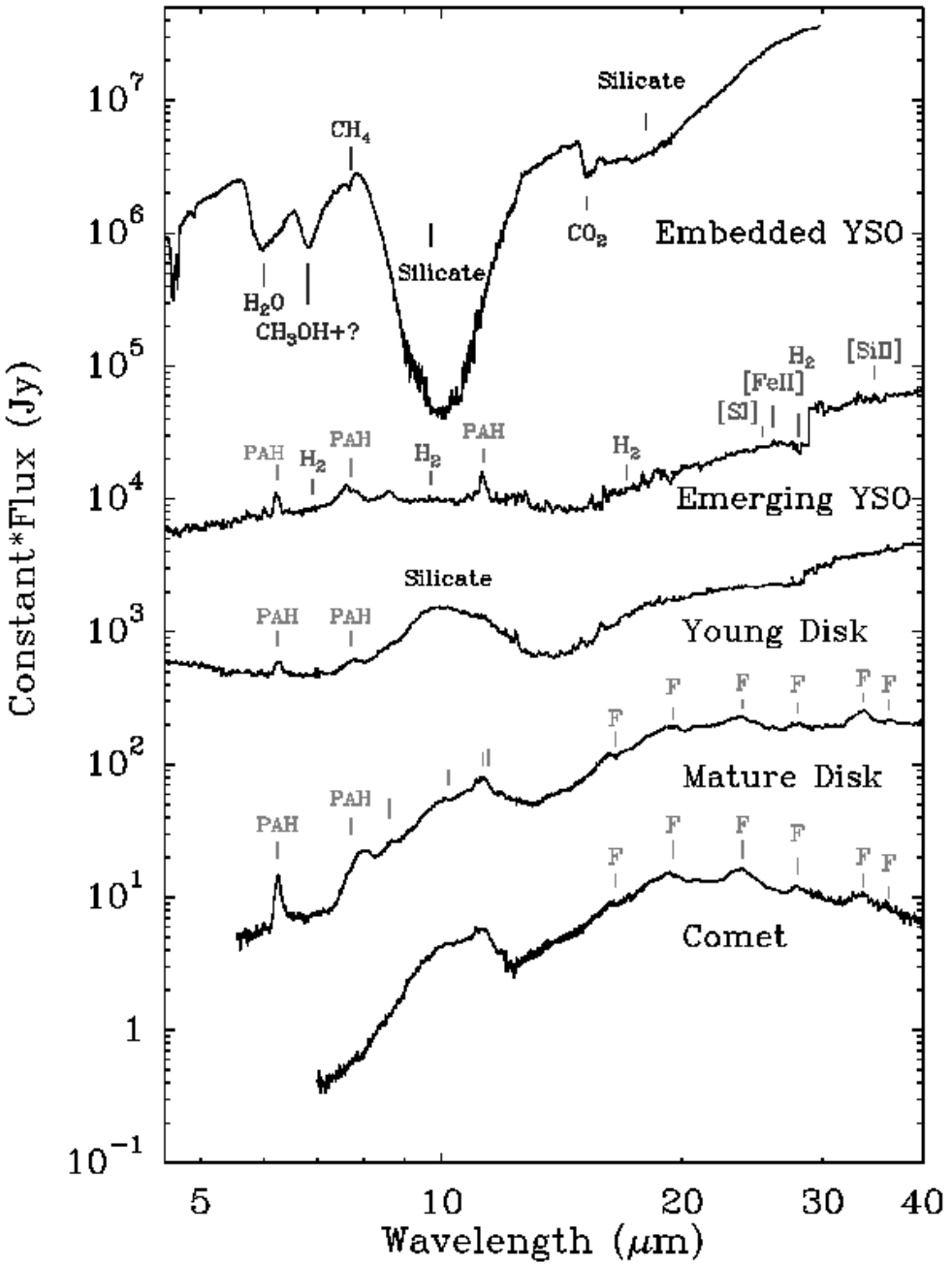

Figure 9.36– ISO-SWS spectra of a range of young stars of different ages and of Comet Hale-Bopp. Sources increase in age toward the bottom.

in circumstellar disks, that is, to the evolution toward mature planetary systems, but little is presently known about how this transformation from amorphous to crystalline silicate material occurs. The amount of material that is processed in this fashion is also unclear.

Emission from "Molecular-Sized" Carbonaceous Grains

Infrared observations of regions of moderately dense gas exposed to intense UV radiation fields, called Photon Dominated Regions or PDRs, in the 1970s and 1980s revealed bright emission features at 3.3, 6.2, 7.7, 8.6, and 11.3 μm (Figure 9.37). First called the Unidentified InfraRed features (UIRs), a host of carriers was proposed. From spectra such as those outlined above, it is now widely accepted that these features arise from a class of molecules related to Polycyclic Aromatic Hydrocarbons (PAHs). The features are bright even far from the illuminating stars; hence the emission process must be non-thermal in nature where the absorption of a single UV or FUV photon can create internal temperatures of nearly 1000 K. We'll look more at how this process works once we cover the electronic spectroscopy of molecules. Here we simply note that the energy considerations dictate molecules some 50-100 C atoms in size, and that the general appearance of the spectrum demands that the material be largely aromatic. Because the spectra are a blend of many species and not rotationally resolved, spectra such as that presented below cannot be used to determine individual carriers.

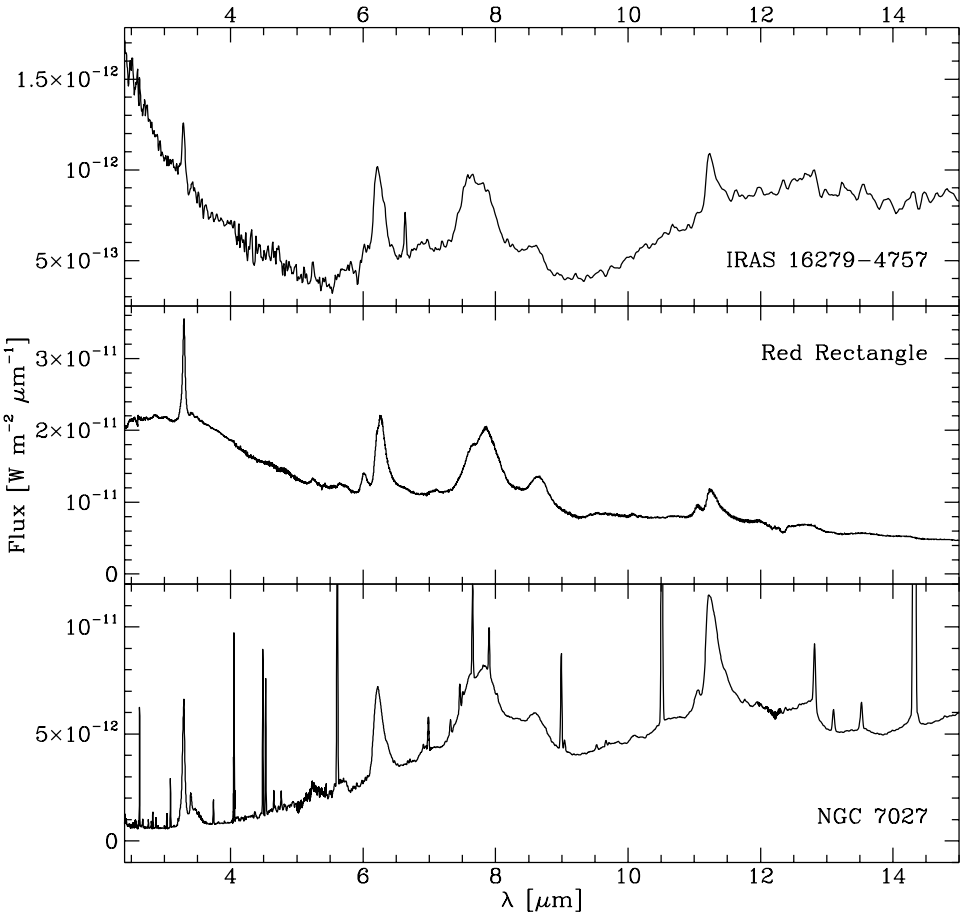

Figure 9.37– The 3-15 μm ISO-SWS spectrum of two post-Asymptotic Giant Branch (post-AGB) stars, IRAS 16279-4757 and the Red Rectangle, and that from the planetary nebula NGC 7027. These UIR features arise from large aromatic molecules that are excited by optical and UV photons.